HUBS White Paper: Galactic Science

March 2023

Galactic sciences play a crucial and indispensable role in Astrophysics, by providing the nearest targets for detailed study of the interstellar medium, energetic explosions, stars, compact objects, etc. The diffuse hot plasmas in our Galaxy are mainly contributed by X-ray diffuse gas, supernova remnants, stellar activities, and also emission from our Solar systems.

1 Cosmic X-ray Background

Contributors: Hang Yang, Zhijie Qu, Wenhao Liu, Shuinai Zhang, Guiyun Liang, Li Ji, Chao Geng, Xuan Fang

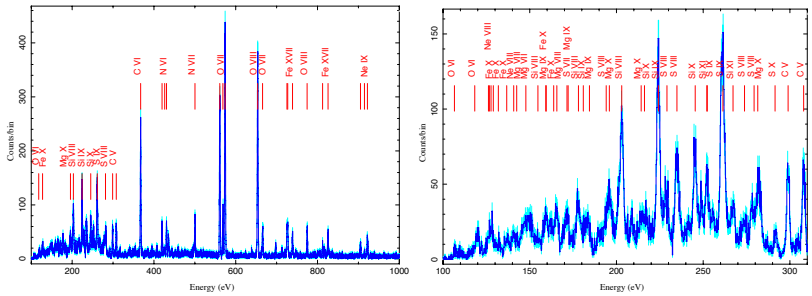

Figure 1: The mock HUBS spectrum of the CXB with an exposure of about 12 ks, based on the model from McCammon+2002.

1.1 General description

The cosmic X-ray background (CXB) was one of first discoveries of X-ray astronomy, along with the first extrasolar X-ray source Scorpius X-1 (Giacconi et al. 1962). (This was even well in advance of the discovery of the cosmic microwave background by Penzias & Wilson (1965), making it the first cosmological diffuse flux ever observed.) Later the flux level of the soft X-ray band ($44 - 70$ Å) was successfully measured by Bowyer et al. in 1968 and Bunner et al. in 1969, and interpreted as truly diffuse emission of hot plasma (Weymann 1967; Henry et al. 1968).

Our understanding of the soft X-ray background has progressed considerably in the ensuing more than 50 years, with generations of X-ray instruments. The diffuse cosmic X-ray background (CXB) has been explored with generations of X-ray telescopes, e.g., HEAO-1 (Gruber+99), RXTE (Revnivtsev+03), BAT (Ajello+08), Swift (Moretti+09), and Chandra (Cappelluti+17).

Aside from the in-service all-purpose telescopes such as *Chandra* X-ray observatory (CXC, ref TBA) and *XMM-Newton* (ref TBA), as well as retired ones as *ROSAT* and *Suzaku*, many kinds of space missions have been dedicated to probe the nature of the soft X-ray background. Recent missions include the space shuttle payload "Diffuse X-ray Spectrometer" (DXS, Sanders et al. 2001), dedicated explorer "*Cosmic Hot Interstellar Plasma Spectrometer*" (*CHIPS*, Hurwitz et al. 2005), and sounding rocket mission "Diffuse X-rays from the Local galaxy" (DXL, Galeazzi, M., et al. 2011, 2014). Their performance is summarized in tab:CXBmissions.

In general, the CXB can be decomposed into two kinds of origins, galactic and extragalactic. The galactic soft X-ray emission consists of three distinct components, the solar wind charge exchange

Table 1: Performance of space missions dedicated to the SXRB studies

Parameters	ROSAT	DXT	CHIPS	Suzaku	DXL	HUBS	XRISM
Launch time	1990.06	1993.01	2003.01	2005.07	2012.12	-	-
Energy Range (keV)	$0.1-2.4$	$0.15-0.28$	$0.05-0.14$	$0.2-12$	$0.11-0.284$	$0.1-2.0$	$0.3-12$
$R=E/\Delta E$	1.2 @0.25 keV	$25-40$	$45-155$	~ 10 @0.5 keV	~ 250 @0.5 keV	≥ 900 @6 keV	
Grasp* (cm2 sr)	~ 0.2 @0.2 keV	0.015 @0.18 keV	0.0007 @0.07 keV	~ 0.01 @1.5 keV	~ 3.5 @0.25 keV	0.15 @1 keV	0.0001 @1 keV

(SWCX), the Local Hot Bubble (LHB), and the galactic halo, while the extragalactic origin is dominated by AGNs. Distinguishing these components from each other and quantifying their contribution to the soft CXB are limited by the spectral resolution of current space missions and model dependent. For example, there was debate on whether the observed soft X-ray emission at 1/4 keV was due to LHB or purely from SWCX (e.g., Lallement 2004; Koutroumpa et al. 2009; Robertson et al. 2009). However, its characteristics requires further study, e.g., the proportion of LHB to the 1/4 keV flux as well as its pressure equilibrium to the local interstellar clouds (Snowden et al. 2014, ApJL), and a proper model that conforms with observed line flux is also under-investigation. In contrast, current space missions are of limited performance to carry out detailed investigation. Most of them are lack of spectral resolution that meets the requirement of line diagnosis.

Future missions with higher spectral resolution, such as HUBS, can provide unprecedented line diagnostics to help understand the origin of the CXB. On the other hand, both in-service and past missions barely cover the 0.1-0.5 keV band, which seems to be a turnover in the spectral energy distribution of cosmic UV/X-ray background (HM12, KS19, FG20). With HUBS, we can obtain finer constraints on the UV/X-ray background modeling.

1.2 Components

1.2.1 Local bubble

It has been identified that the solar system resides in a cavity of low-density and ionized gas, surrounded by a shell of cold neutral gas and dust. The existence of such a cavity was implied by the soft X-ray emission seen in the ROSAT map at 1/4 keV (Snowden+97), and was dubbed as the "local hot bubble" (Sanders et al. 1977, Cox et al. 1987). Though debates on the model exist, the LHB still led its popularity and was strongly supported by recent studies (Snowden et al. 2015a, 2015b). Many of the following researches also pay attention to its irregular shape and extent, suggesting a pathlength of order 100 pc (Lallement et al. 2013, Snowden et al. 2014, Liu et al. 2017, Zucker et al. 2022), possibly created and maintained by stellar winds or supernova explosions due to nearby star formation activities.

Despite the change in intensities with respect to latitudes, soft X-ray emission from the LHB can be characterized by a hot phase plasma with $T \sim 0.1$ keV (Truemper et al. 1982, Sanders et al. 2001, Wulf et al. 2019). However, possible contamination arises from foreground SWCX, and galactic halo at intermediate and high latitudes.

X-ray shadowing method is invoked to divide the observed emission into foreground and background components (Snowden et al. 2015a, Uprety et al. 2016). Based on the DXL data, Liu et al. (2017) removed the contribution by SWCX and reported a uniform temperature $k_{\rm B}T = 0.097 \pm 0.013$ keV, slightly cooler than previous results. Modeling SWCX has been progressed as well. New models to calculate charge exchange emission in X-ray band, including the most recent atomic data and a complete transition calculation, have been implemented in Xspec and SPEX, respectively by two groups (e.g., Smith et al. 2014; Gu et al. 2016), but lack of the detailed information about the solar wind abundance and the ionization state, and the theoretical and experimental cross sections.

Not only will HUBS provide better constraints on the portion of SWCX in the CXB, but also help to understand the galactic halo.

1.2.2 Galactic halo

The gaseous halo (also known as the circumgalactic medium; CGM) is a fundamental component surrounding the galaxy, which is deeply involved in galaxy evolution by regulating the gas assembly and gathering feedback from the galaxy (see recent reviews Tumlinson et al. 2017; Donahue and Voit 2022). In the past three decades, extensive efforts in observations supported that the total mass of the CGM can be as massive as the stellar content in the galaxy (i.e., $4-10\times10^{10}M_{\odot}$ for L_* galaxies; e.g., Werk et al. 2014; Bregman et al. 2018). Furthermore, multi-wavelength observations revealed the multiphase nature of the CGM, covering a wide range from the dust and molecular gas (10-100 K; Menard et al. 2010; Muzahid et al. 2016), neutral gas ($T\lesssim10^4$ K; Tumlinson et al. 2013), photoionized cool-warm gas ($T\approx10^{4-5}$ K; e.g., Zahedy et al. 2019; Qu et al. 2022), to collisionally ionized hot gas (e.g., X-ray emitting; $T\sim10^6$ K; Bogdan et al. 2015; Li et al. 2018). The Milky Way (MW) is of particular interests because it not only has the most complete multi-wavelength observations in most bands, but also the best known stellar evolution (especially around the solar neighbor) to study the impact of the galaxy on its CGM.

The gaseous halo of the MW has been known to have complex structures in spatial distribution together with the multi-phase temperature or ionization state distribution (see Putman et al. 2012 for a review). Particularly, the neutral and low ionization state gas are found to be separate clouds beyond the Galaxy disk, which can be identified by their velocities ($|v_{LSR}|\gtrsim100$ km s^{-1}; known as high-velocity clouds, HVCs; e.g., Wakker and van Woerden 1997). These low ionization state clouds are predicted to have two origins, condensed from the hot gaseous halo or ejected from the disk by feedback, which may be accreted again as recycled gases (e.g. Fraternali 2017). Once they are formed, these clouds continuously interact with the ambient hot gas in the halo, which further generates the intermediate ionization state gases (i.e., traced by C IV or O VI). Therefore, the hot gas is a crucial component of the baryonic cycle in the gaseous halo, participating formation and evolution of multiphase gases.

The hot gasesous halo was firstly predicted by Spitzer (1956), while the first hint of the hot gaseous halo was observed by the RASS (Truemper 1982). With a resolution of 2°, complicated spatial structures have been found over the entire sky, with a clear anti-correlation is observed between the soft x-ray emission (1/4 keV) and the neutral hydrogen (e.g., Snowden et al. 1995). Such an anti-correlation implies a distant origin of the diffuse soft x-ray emission, which includes the contribution from the hot gaseous halo of the MW. It was implied by the anti-correlation between the soft X-ray emission at 1/4 keV and the neutral hydrogen (e.g. Snowden et al. 1995). After ROSAT, high spectral resolution spectra obtained by Diffuse X-Ray Spectrometer (DXS) aboard the sounding rocket revealed that the soft x-ray emission was dominated by thermal emission of hot gas ($k_{\rm B}T\approx0.1-0.2$ keV), which favored a galactic halo origin (McCammon et al. 2002). Furthermore, the launch of flagship telescopes XMM-Newton and Chandra further enabled high spatial resolution observations to decompose the diffuse contribution seen by ROSAT into the extragalactic point sources (e.g., AGN; Hornschemeier et al. 2000) and truly diffuse emission.

In the past two decades, the understanding of the Galactic hot halo has been improved a lot by deep XMM-Newton and Chandra observations in both emission and absorption. Particularly, the spatial distribution of the MW hot halo has been established as the first order approximation assuming the spherical symmetry (e.g. Henley and Shelton 2012; Gupta et al. 2012; Miller and Bregman 2013). Furthermore, the temperature distribution of the hot halo has been investigated, showing another extreme hot phase at $k_{\rm B}T\approx0.7$ keV (e.g., Das et al. 2019a). In the current decade, newly launched surveyors eROSITA and HaloSat also continuously provide new insights, such as the discovery of the soft x-ray bubbles in both sides of the MW (i.e., eROSITA bubbles; Predehl et al. 2020).

Although it has been an astounding progress to understand the Galactic hot halo from decades ago, there are still fundamental open questions in the field. For an instance, the metallicity of the hot halo is still controversial. On one hand, the continuum of the thermal emission due to the Galactic hot halo is hard to be decomposed from other contributors to the continuum (e.g., the CXB or the soft proton), limited by the relatively poor spectral resolution of the existing instruments. On the other hand, the SWCX contributes to the soft x-ray line emission, which is also blended with the emission of Galactic hot halo. These difficulties make it a hard problem to determine the hot halo metallicity. The high resolution and spectral coverage down to 0.1 keV of HUBS could bring new possibilities to determine the metallicity by clearly decomposing line emission and continuum or determining the line ratios between forbidden and resonant lines.

Another intriguing question is about the potential extremely hot phase in the Galactic halo. Currently, detection of an extremely hot phase at $k_{\rm B}T \approx 0.7$ keV has been claimed in both emission and absorption. However, these evidences have limitations in different ways. The absorption line analyses rely on weak detection ($\approx 2-3\sigma$) of Ne IX and Ne X in two sight lines (Das et al. 2019a, 2021). The modeling of this absorption system requires both super high temperature and super solar neon abundance of [Ne/O] ≈ 0.7, which raise questions about its origin (e.g., in the Galactic disk or the Galactic halo). The emission evidence of the super hot component is mainly the unexpected enhanced feature at 0.8-0.9 keV in the single temperature hot halo model. However, as suggested in Wulf et al. (2019), the similar feature observed at low Galactic latitudes can be explained by the hot corona of M dwarf stars in the disk. Adopting the 2 models in Wulf et al. (2019), M dwarf stars can contribute $\approx 2-4\times10^{-7}$ kpc cm^{-3} at high latitudes, which can be 50 - 100% of the claimed detection of extremely hot phase (e.g., Das et al. 2019b; Bluem et al. 2022). The high spectral resolution and relatively high spatial resolution of HUBS could provide unique insights into the extreme hot phase by constraining line ratios (determining radiation mechanisms) and resolving possible M dwarfs in the field. Therefore, although HUBS is not a dedicated surveyor focusing on the diffuse emission of the Galactic hot halo, its unique combination of large FOV and high spectral resolution opens a special window to study the Galactic hot halo.

1.2.3 Extragalacitc sources

While the diffuse Galactic and the local emission dominate the SXRB in the $0.5-1$ keV band, the majority of the X-ray background has been recognized as discrete extragalactic sources, mostly AGN and star-forming galaxies. According to the deepest observations by Chandra and XMM-Newton, in the $0.5-2$ keV band, the resolved fraction of the extragalactic background reaches about $80-90\%$ (e.g., Moretti et al. 2003; Worsley et al. 2005; Hickox and Markevitch 2006; Lehmer et al. 2012; Xue et al. 2012). As a consequence, insights into the extragalactic background may serve as a constraint on the integrated SMBH growth and the accretion physics of galaxies.

However, there still remains unresolved SXRB of unknown origin, for e.g., about 10% diffuse emission in the 1-2 keV band (Hickox and Markevitch 2007). It may be from CGM of galaxies within their Virial radii (Mineo et al. 2012) or "warm-hot" intergalactic medium with temperature of 10^{5-7} K (WHIM; Cen & Ostriker 1999). On the other hand, with current CCD energy resolution, some models for the components of SXRB are over simplified, for e.g., a single-T APEC model for describing the local thermal-like emission cannot interpret the emission excess of SXRB below 0.5 keV (Hickox and Markevitch 2006). Consequently, the uncertainties of the AGN contribution is larger in the $1-2$ keV band, which is essential for disentangling the obscured and the unobscured AGNs (e.g., Treister et al. 2009).

HUBS has a large field of view ($\sim$ 1 squre degree), and therefore most observations will partly cover the region of SXRB, with a remarkable effective area ($\sim$500 cm^2). The X-ray integral field units in HUBS cover the $0.1-2$ keV band which is complementary to the bands of Chandra or the future Athena, and together can give better constraints on the composition of XRB. With the 2 eV high energy resolution, the local diffuse emission can be exclusively determined, and the obscured fraction of AGNs would be more precise. Taking that HUBS is designed for observing CGM and WHIM (e.g., Zhang et al. 2021), it will quantitatively predict their contributions in the SXRB and fill the final gap of the unresolved SXRB.

1.2.4 Solar wind charge exchange

Another important component in the soft diffuse X-ray background is solar wind charge exchange (SWCX) emission. SWCX is generated when the highly charged solar wind ions interact with the neutral materials within the solar systems, gaining an electron in a highly excited state which then decays emitting an X-ray or UV photon with the characteristic energy of the ion. The spectrum of SWCX contain rich emission lines, some of which are also utilized in astrophysical line diagnostics. On top of that, the ubiquity of SWCX makes it a significant contaminant to every X-ray observations of astrophysical objects. Cravens (1997) first proposed charge exchange between the cometary neutrals and solar wind ions as the emission mechanism for the soft X-ray emission detected from Comet Hyakutake (Lisse et al. 1996). It was first proposed to explain the cometary soft X-ray emission (Cravens 1997), and then identified as the source of the long term enhancements observed in the ROSAT

All-Sky Survey (RASS; Snowden et al. 1994, 1995). It was soon realized that long term enhancements, the temporally variable signals observed in the ROSAT All-Sky Survey (RASS) (Snowden et al. 1994, 1995), were due to the solar wind interaction with the neutrals in the Earth's atmosphere (Cravens et al. 2001).

Based on the target neutrals, there are in general two kinds of SWCX, i.e., the geocoronal SWCX and the heliospheric SWCX. The former is due to the interaction between the compressed solar wind ions in the magnetosheath and the neutrals (mostly hydrogen) in the exosphere of the Earth. Hence, its strength and location depends strongly on the strength of the solar wind. The strength and the location of this emission depends strongly on the strength of the solar wind. The latter, on the other hand, is due to the interaction between the free-flowing solar wind and the neutral ISM within the entire heliosphere ($\sim$ 100 AU). Heliospheric SWCX shows direction dependence as a consequence of the structured solar wind and the neutral distribution in the heliosphere, but little temporal variation because of the average effect along the line of sight. Due to the structured solar wind and the neutral distribution in the heliosphere, the heliospheric SWCX emission is direction dependent and shows a small temporal variation due to the average effect along the line of sight.

Due to its ubiquity, SWCX emission contaminates every X-ray observations of astrophysical objects. In particular, the spectrum of SWCX contains rich lines, some of which are also utilized for diagnostics of astrophysical plasma. The inclusion of SWCX emission could significantly change the derived plasma temperature of astrophysical object, and/or mimic a separate diffuse soft X-ray component. For example, there was controversy over the existence of the LHB caused by SWCX emission. Some studies suggested that some or nearly all of the diffuse X-ray emission at 1/4 keV in the Galactic plane was from SWCX (e.g., Lallement 2004; Koutroumpa et al. 2009; Robertson et al. 2009). By measuring the broad-band SWCX emissivity in helium focusing cone using sounding rocket mission, Galeazzi et al. (2014) found that the total SWCX contribution is $\sim$40% of the X-ray flux at 1/4 keV in the Galactic plane.

Despite the difficulties in distinguishing SWCX emission from that of astrophysical plasma, a number of groups have been working to characterize and model SWCX emission. Koutroumpa et al. (2006, 2007) developed a simple model to calculate heliospheric SWCX emission along line of sight, based on the solar wind conditions, interplanetary neutral distributions, and theoretical interaction cross sections. The model has been used to predict SWCX emission in X-ray observations (e.g., Koutroumpa et al. 2009; Koutroumpa et al. 2011; Ringuette et al. 2021), and sometimes there are large discrepancies between the model prediction and the observational results. Similarly, there are models developed to estimate the geocoronal SWCX emission (e.g., Carter et al. 2010; Kuntz et al. 2015). In addition, new models to calculate charge exchange emission in X-ray band, including the most recent atomic data and a complete transition calculation, have been implemented in Xspec and SPEX, respectively by two groups (e.g., Smith et al. 2014; Gu et al. 2016). However, to obtain high-resolution spectra, both models use some approximations to redistribute cross sections, which have limited experimental data or only theoretical calculations. In summary, the largest uncertainties of these models are mainly due to the lack of the detailed information about the solar wind abundance and the ionization state, and the theoretical and experimental cross sections.

HUBS has the unprecedented spectral resolution of 2 eV, which can resolve most of fine-structure lines. Owing to its high spectral resolution, HUBS will allow us to resolve most of the fine-structure lines, which suits well for learning SWCX. It is very suitable for study of SWCX. In principle, line ratios of SWCX emission are different from those in astrophysical plasma emission, e.g., O VII triplets. The HUBS spectroscopy will help to distinguish and separate SWCX emission from the thermal components, e.g., from the LHB, the galactic halo and other distance components.

Due to the low-Earth orbit, HUBS observation will be inevitably affected by the geocoronal SWCX. One strategy to study the SWCX in the near-Earth environment is through HUBS observations of the Moon. HUBS observation will cover the full Moon with its field of view and clearly resolve the SWCX lines with its superior energy resolution (see Fig. 2). On the bright side, strong fluorescence lines from O, Mg, Al, and Si can serve as a remote sensor of the element composition on the lunar surface. While the observation of the dark side of the Moon will maximize the SWCX signal by blocking the thermal emission from our galaxy and distant objects. The X-ray emission from the dark Moon mainly consists of two parts: the emission from the magnetosheath (the near-Earth environment $< 10\ R_E$) and from the region between the bow-shock ($\sim 10\ R_E$) and the Moon (60 R_E). For the near-Earth environment, the high variability of SWCX is complicated by the solar wind temporal variation. Real-time monitoring

of the solar wind is necessary for accurate data analysis. In-situ measurements from ACE [1] and/or the future Chinese space mission SMILE [2] will provide valuable data. Another important factor in the SWCX luminosity is the neutral distribution in the magnetosheath, which requires sophisticated magneto-hydrodynamic modeling for the solar wind interaction with Earth's atmosphere [**Sun2020**]. The high-resolution spectra obtained by HUBS will precisely measure the SWCX contribution in the near-Earth environment and help to test the results of MHD models. In addition, data can be used to constrain the charge exchange cross-sections measured in the laboratory. Meanwhile, it also requires the laboratory measurements to improve the current charge exchange models.

2 Supernova remnants

Contributors: Lei Sun, Ping Zhou, Yang Chen, Fangjun Lu, Ziwei Ou, Wei Sun, Xuejuan Yang, Xin Zhou

Supernovae (SNe) are among the most violent explosions in the universe, which release a typical energy of $\sim 10^{51}$ erg in a rather short timescale. As an essential part of the galactic ecosystem, SNe play an important role in the baryon cycle and the energy feedback. Supernova remnants (SNRs) are SNe interacting with the surrounding circumstellar material (CSM) and interstellar medium (ISM), which provide an important mean to study the physics of both sides of the interaction.

SNRs are bright sources in the X-ray sky and the nearest targets to constrain how SNe influences galactic ecosystems observationally. Over a hundred X-ray-bright SNRs have been found thus far in our Galaxy, LMC, and SMC. These extended sources are actively heating the interstellar medium with fast shocks and enriching it with heavy elements. The X-ray observations in past decades have greatly advanced our knowledge on SNRs [103], but also post some challenges that require X-ray observations with high spectral resolution.

Some crucial questions in SNRs are yet to be answered with future X-ray instruments with high spectroscopic capabilities: 1) What are the metal compositions in diverse SNRs and how do different supernovae contribute to producing heavy metals in our Universe? 2) How are the hot plasmas in non-equilibrium ionization produced? 3) How to constrain charge exchange and resonant scattering processes using emission lines? 4) How is the kinematics of the ejecta/CSM connected to the SN explosion mechanism and the progenitor system, and how does collisionless shock heat up different particle species? 5) What are the X-ray SNR populations in nearby galaxies? Below we summarize why HUBS will help us address these key questions.

2.1 Associate SNRs with their progenitors

One of the major challenges in the SNR study concerns identifying the progenitor type. The two major types of SNe — the core-collapse SNe and the Type Ia (thermonuclear) SNe — can be well-defined and easily distinguished based on their optical spectrum around maximum light. However, it is not that straightforward to associate an evolved SNR with its original progenitor system, which needs a detailed investigation into the properties of the SN ejecta and the CSM.

Type Ia SNe represents the thermonuclear explosions of C/O white dwarfs. The nuclear burning in Type Ia SNe typically results in a large amount of iron-group elements (IGEs) suchs as Fe and Ni as well as intermediate-mass elements (IMEs) such as Si, S, Ar, and Ca [53, 85]. However, in the case of core-collapse SNe, one may expect oxygen as the major product of the nucleosynthesis [67, 89]. Therefore, the SN ejecta metal abundances (or abundance ratios) can be used as diagnostics for typing their remnants [115]. SNRs showing evidence of enhanced oxygen abundances (so-called oxygen-rich SNRs) are commonly considered from the core-collapse explosions of the most massive stars, while SNRs dominated by IGEs and IMEs are more likely from Type Ia events. The X-ray spectra of SNRs contain most of the prominent emission lines from these metal species, which are essential for constraining the ejecta properties. However, the X-ray spectra of SNRs can always be a combination of the non-thermal emission from the accelerated particles and the thermal emission from the shocked ejecta and CSM/ISM. Therefore, a precise measurement of the metal abundances relies on high-resolution X-ray spectroscopy that allows us to separate, identify, and measure the individual

[1] https://solarsystem.nasa.gov/missions/ace/in-depth/
[2] http://english.cssar.cas.cn/smile/

emission lines, and to distinguish the ejecta from other components. This can be challenging for the CCD instruments. For example, with a typical energy resolution $\Delta E \sim 100\,\mathrm{eV}$, CCD instruments can hardly resolve the Fe-L complex and the Ne Heα lines around ~ 0.7–$1.0\,\mathrm{keV}$, which will be seen as a bump-like structure or a pseudo-continuum and lead to large uncertainties in the measured abundances. The current grating instruments such as XMM-Newton RGS and Chandra LETG/HETG may partially solve this problem, but they are limited to those bright remnants with small angular sizes and the remnants with bright knot/filament structures.

The constraint on the X-ray properties of the shocked plasmas in SNRs, and our understanding of the SN-SNR connection, will be significantly improved with the help of HUBS. The HUBS energy band (0.1–2 keV) covers most of the He-like and H-like emission lines from C, N, O, Ne, Mg, Si, and L-shell emission lines from Fe and Ni. With an ultra-high energy resolution of $\sim 2\,\mathrm{eV}$ of the main array and $\lesssim 1\,\mathrm{eV}$ of the central sub-array, HUBS is capable of resolving individual emission lines, especially the He-like triplets (i.e., the resonant lines, the forbidden lines, and the intercombination lines) and the Fe-L complex. On the other hand, the spatial resolving ability and the large field of view may help to map the spatial distributions of the plasma parameters over the whole remnant.

Potential HUBS target for this topic could be any SNR that is emitting X-rays and not subjected to heavy absorption. We briefly summarize some of them below.

2.1.1 Kepler's SNR

Kepler's SNR (G4.5+6.8, Kepler in short hereafter) is the remnant of the latest historical supernova SN 1604 (also known as Kepler's SN), and is one of the best-studied SNRs in our galaxy. Its historical light curve, and its location (high above the galactic plane with $b = 6.8^\circ$), together with its Fe-dominated X-ray spectrum, suggest that Kepler originated from a Type Ia explosion. However, as a Type Ia remnant, Kepler exhibits significant features of the shocked CSM, making its progenitor system unique. Given the large amount of the shocked CSM, Kepler is very likely from a single-degenerate system, where a CO white dwarf accretes mass from a non-degenerate donor star until it reaches the Chandrasekhar limit. Based on the total mass and the nitrogen-rich abundance of the CSM, the donor star is suggested to be an asymptotic giant branch (AGB) star [11, 91]. Nevertheless, there are still a couple of problems regarding the progenitor system and the explosion mechanism of Kepler. First of all, a previously luminous massive donor star should be able to survive the explosion and is likely still bright enough to be detected. However, no such survival donor star has been discovered so far. This is not only a problem for Kepler but for any SNR considered a single-degenerate system. One possible solution to this problem is the so-called core-degenerate scenario, where the single-degenerate system forms a common envelope at the final stage of its evolution and the merging of the white dwarf with the secondary star core eventually induces the explosion [97]. This scenario may also help to explain the two "ears" of Kepler which can be caused by pre-explosion jets [97, 91]. Another question is how the bow-shock-like CSM structure was formed. This feature indicates that the progenitor system of Kepler may have a high bulk velocity $\sim 250\,\mathrm{km\,s^{-1}}$ away from the galactic plane [4, 2, 86], which means a runaway binary system. Such kind of system is rare according to nowadays observations. Only a few examples are known (e.g., the Mira system which has a velocity of about $100\,\mathrm{km\,s^{-1}}$ and consists of an AGB star and a probable white dwarf [56]).

HUBS can help to improve our understanding of Kepler. Figure 3 shows a simulated 100 ks central array spectrum of Kepler. The central array of HUBS has a field of view $\sim 3' \times 3'$ which may enclose most of the remnant, and its ultra-high energy resolution provides a clear view of the emission lines. As seen in Figure 3, emission lines from various metal species are detected and well separated — among which the N, O, Ne, and Mg lines are mainly from the shocked CSM while the Fe and Si lines are dominated by the shocked ejecta material. Therefore, HUBS provides us an opportunity to perform the spectroscopic study in great detail, distinguish the CSM and the ejecta components, and constrain their properties individually. The abundances and kinematics of the CSM are essential in indicating the progenitor system, while the abundance pattern of the ejecta is also important for determining the explosion mechanism.

2.1.2 Puppis A

One of the promising targets for HUBS on this topic could be Puppis A.

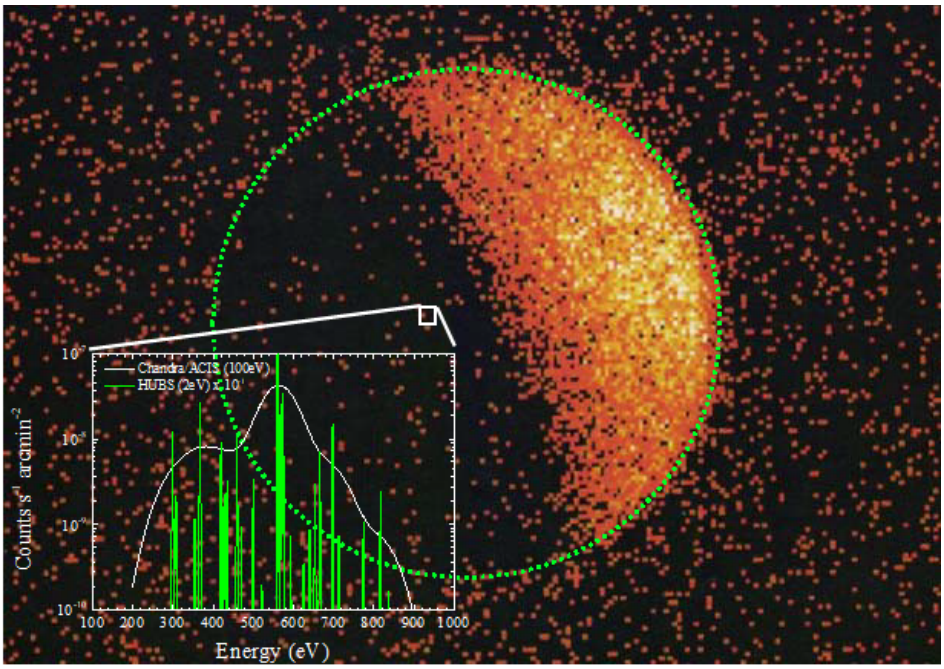

Figure 2: The PSPC observation for the Moon [**Schmitt1991**], inside panel shows the simulation (2 eV, green curve) for an average slow solar wind (v =400 km/s) at one chip marked by open white box along with the comparison to /ACIS simulation (100 eV, white curve). Here, the CX model uses the same exospheric hydrogen as in previous work [**Wargelin04**].

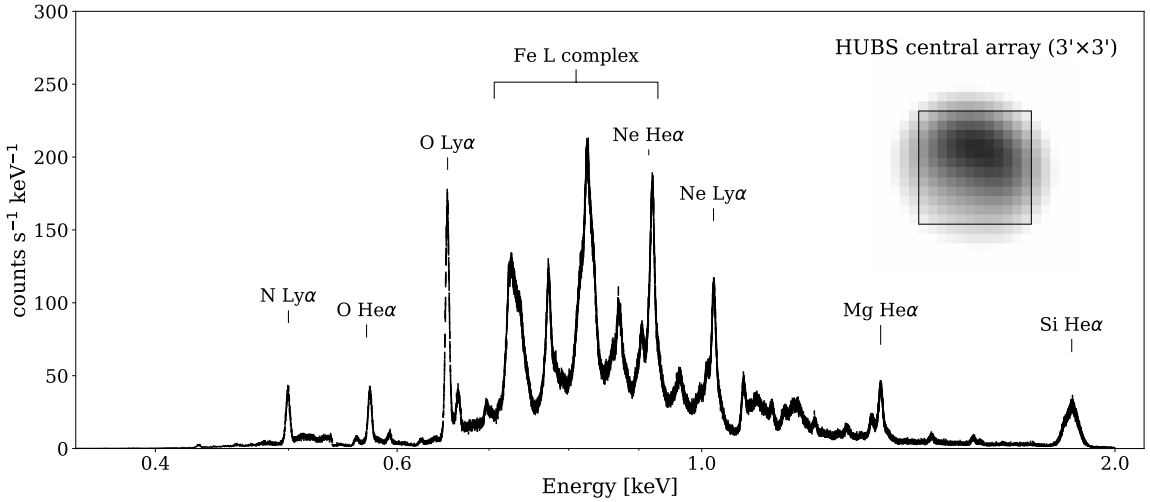

Figure 3: Simulated 100 ks HUBS central array spectrum of Kepler's SNR. Great numbers of emission lines from various elements and ions can be detected and well separated by HUBS. At the upper right corner, we show the simulated HUBS central array image of Kepler, with the black box denoting the field of view of the central array ($\sim 3' \times 3'$).

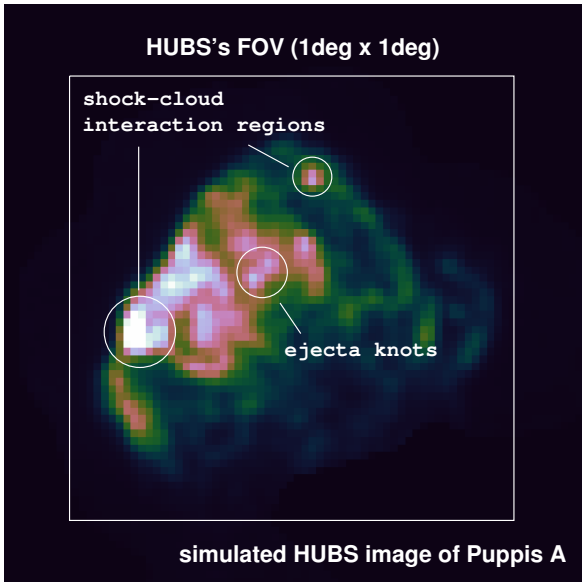

Figure 4: Simulated HUBS image of Puppis A, with the white box denotes the HUBS's field of view ($\sim 1^\circ \times 1^\circ$).

Puppis A (G260.4−3.4) is a nearby Galactic SNR (recent H I absorption study suggests a distance to Puppis A as 1.3 ± 0.3 kpc [81]), and is among the brightest SNRs in X-rays. Due to its relatively large angular size ($\sim 56'$ in diameter), for most of the existing X-ray instruments such as XMM-Newton EPIC and Chandra ACIS, we have to make multiple observations with different aim points to cover the whole remnant. However, the large field of view ($\sim 1^\circ \times 1^\circ$) of HUBS may perfectly enclose the majority of the remnant in a single observation, providing spatially-resolved high-energy resolution spectroscopic data of Puppis A.

Figure 4 presents a simulated HUBS image of Puppis A. Puppis A belongs to the so-called "oxygen-rich" SNRs which show prominent oxygen emission in the optical band and hosts the central compact object (CCO) RX J0822–4300. Therefore, it is recognized as one of the typical remnants originating from a core-collapse explosion of a massive star. However, the X-ray emission of Puppis A is predominated by the shocked interstellar medium (ISM), while the presence of an ejecta-dominated clump has been noticed and studied recently using the XMM-Newton, Suzaku, and eROSITA observations [37, 30, 40, 58]. Our understanding of the progenitor is still limited.

HUBS may help us further investigate the physical property and distribution of the shocked ISM, especially its peculiar NE-SW gradient. More importantly, HUBS can obtain the high-resolution spectra of the ejecta clumps, which is essential in measuring the metal abundances and inferring the progenitor mass.

Except for Kepler and Puppis A, other promising targets include Cas A, Tycho, SN 1006, etc., which are all X-ray bright young SNRs and have been taken as the typical remnants of their kind. For example, Cas A is one of the best-studied SNRs and has been taken as the first-light source and calibration source for many X-ray telescopes. It is a Type II remnant with a CCO. It has a complicated but fascinating ejecta structure with multiple ring-, jet-, bubble-, and even donut-like features [61, 62]. It belongs to the oxygen-rich remnants, and its progenitor mass is estimated to be 16–20 $M_\odot$ [10]. Tycho's SNR is the remnant of SN 1572, a Type Ia event. Like Kepler, Tycho could also come from a single-degenerate system: A survival donor star candidate identified for Tycho [82], but its identification is disputed [45]. The remnant is in an expanding molecular cloud bubble, which can be produced by strong progenitor winds in a single-degenerate system[116]. SN 1006 provides another example of a Type Ia remnant, which is evolving in a tenuous ISM environment. Unlike other young SNRs such as Cas A, Tycho, and Kepler, the X-ray spectrum of SN 1006 is dominated by the non-thermal synchrotron emission from the two limbs. The interior of the remnant does show faint thermal features. However, since the reverse shock has not yet reached the inner Fe-rich ejecta, the

thermal emission is dominated by O, Ne, Mg, and Si lines but has few Fe features [49].

HUBS can help us to carry out detailed spectroscopic studies on all of SNRs mentioned above and provide further clues to their progenitor systems and explosion mechanisms.

2.2 Constrain the origins of non-equilibrium ionization plasmas

At the early phase of the SNR evolution, due to the low density of the shocked plasma, the ionization process may take a rather long timescale before reaching equilibrium ($n_e t \sim 10^{12}\,\mathrm{cm^{-3}\,s}$). Therefore, the shocked plasma in young SNRs is expected to be in the non-equilibrium ionization (NEI) state, where the plasma is still under-ionized (ionizing plasma, IP), characterized by an ionization temperature kT_i which is lower than the electron temperature kT_e. The observational evidence for this under-ionized NEI plasmas has been extensively established for a number of young SNRs such as Cas A, Kepler's SNR, SN 1006, SN 1987A, etc (e.g., [102, 79, 91, 49, 92]). However, recent X-ray spectroscopic studies have revealed the existence of over-ionized plasma (recombining plasma, RP) in several SNRs, where kT_i goes even higher than kT_e (e.g., IC 443, G359.1-0.5, W28, W44, etc., [44, 110, 70, 83, 100]). So far, RPs have been found in over a dozen of SNRs, which may represent a new subclass of SNRs [90].

The physical origin of the RPs in SNRs has not yet been fully understood. Theoretically, there are two approaches to an over-ionization state of the plasma: increase of kT_i (extra ionization) or decrease of kT_e (electron cooling). The extra ionization can be caused by suprathermal electrons [70], high-energy photons [44], and low-energy cosmic ray protons [111]. On the other hand, the electron cooling scenario, which is considered to be better applied to the SNR evolution, may arise from adiabatic expansion [32] and thermal conduction [44, 117]. In addition, simulations indicate that various scenarios, such as the adiabatic expansion and the thermal conduction, may simultaneously contribute to the formation of RP [117, 112].

The X-ray emission of RPs is characterized by several distinct spectral features, including the radiative recombination continua (RRCs), enhanced Lyα to Heα line ratios, and enhanced He-like ion G ratios (defined as $G = (f + i)/r$, where r, f, and i stand for the resonant, forbidden, and intercombination line flux, respectively). Limited by the energy resolution of the current CCD instruments, the studies on RPs by far are mostly based on the RRCs and Lyα lines lying in the $\gtrsim 2\,\mathrm{keV}$ band (covers mainly the heavier elements such as Si, S, and Fe), and thus may leave some bias. HUBS will extend our study into the lower energy band (0.1–2 keV), providing greatly-improved observations on N, O, Ne, Mg lines and their RRCs. In addition, the spatial resolving ability of HUBS can help to map the distribution of RPs in SNRs, which is crucial in determining their physical origins.

2.2.1 SNR 3C400.2

SNR 3C400.2 (G53.6−2.2) is one of the few remnants in which people have detected recombining features in the $< 2\,\mathrm{keV}$ band so far [6] (another possible example could be SNR CTB 1 [43]). Same as many other RP-detected SNRs, 3C400.2 belongs to the so-called thermal-composite (or mixed-morphology) SNRs, which contain a thermal X-ray dominated central part and a radio-emitting shell (shown as the left penal in Figure 5). The physical origin of the RP, as well as the formation of its mixed-morphology feature, is still unclear. The presence of RP in 3C400.2 was firstly reported based on Chandra observations in 2015 [6], and then confirmed by Suzaku observations in 2017 [16]. However, the two studies disagree with each other on the physical properties of the RP — Chandra observations indicate the RP has a low temperature ($\sim 0.14\,\mathrm{keV}$) and solar abundances while Suzaku observations suggest an RP component with relatively high temperature ($\gtrsim 0.6\,\mathrm{keV}$) and enhanced abundances. This discrepancy leaves the origin of the RP under debate. Both of these two studies are limited by the relatively poor energy resolution of CCD instruments. The major recombining features, such as the RRCs of Ne and Mg, lie in the $< 2\,\mathrm{keV}$ band, where plenty of emission lines blend with each other and can hardly be separated in the CCD spectrum. Both Chandra and Suzaku can only provide marginal detections of the RRCs and result in large uncertainties in measuring the physical parameters of RP.

With the high-energy-resolution microcalorimeter onboard, HUBS is especially good at catching the delicate features in the soft (0.1–2 keV) X-ray band. In Figure 5, we present a simulation of the 100 ks HUBS spectrum of 3C 400.2. The template model is based on the Chandra observations. We then fit the HUBS spectrum with two different plasma models. As shown in the lower panels of Figure

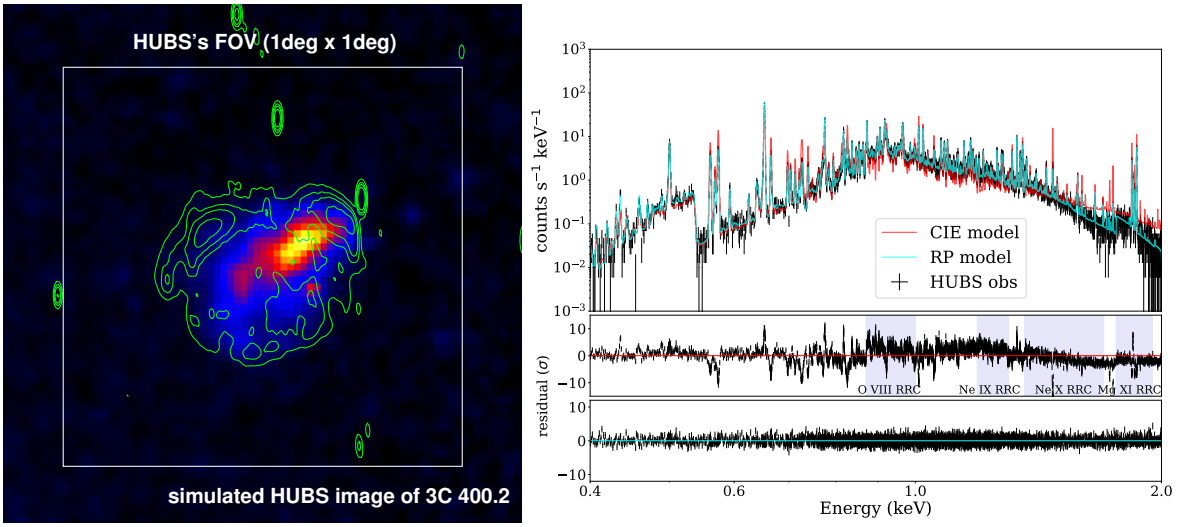

Figure 5: Left: simulated HUBS image of SNR 3C 400.2, overlaid with 1.4 GHz radio contours from the Canadian Galactic Plane Survey (CGPS). The white box indicates the HUBS's field of view ($\sim 1^\circ \times 1^\circ$). Right: simulated 100 ks HUBS spectrum of SNR 3C 400.2 (black data points), fitted with a collisional ionization equilibrium plasma model (CIE model, the red curve) and a recombining plasma model (RP model, the cyan curve), respectively. The lower panels show the residuals.

5, a collisional ionization equilibrium (CIE) plasma model leaves significant residuals at the RRCs of O VIII, Ne IX, N X, and Mg XI, as well as the Heα and Lyα lines, which can be clearly identified with the help of HUBS. A recombining plasma model can perfectly describe the observed spectrum, and provide tight constraints on multiple physical parameters.

Other targets for HUBS on this topic could be W28, W44, IC 443, and other RP-detected SNRs. Although for most of these SNRs, their recombining features are mainly detected at > 2 keV band, such as RRCs of Si, S, and Fe, the obtained RP parameters predict recombining features exist also in the < 2 keV band that the current CCD instruments may fail to detect. HUBS can help to improve the detection of the recombining features in the soft band and the constraint on the overall properties of the RP. On the other hand, other thermal-composite and gamma-ray emitting SNRs are potential sources where we can use HUBS to search for signatures of the RP.

2.3 Diagnose charge exchange and resonant scattering processes

The excellent energy resolution of HUBS is especially suitable for line-oriented studies. Here, we bring up two examples in SNR physics, concerning the charge exchange process and the resonant scattering effect.

Charge exchange (CX) takes place in various astrophysical environments where hot ionized plasma interacts with a neutral gas, such as solar wind interacting with planet atmospheres, comets, and the heliosphere. The collisionless shocks in SNRs provide a promising site for CX study. Right behind the SNR shock front, unshocked cold neutrals may collide with the shocked hot ions and go through the CX processes, resulting in a population of highly excited recombined ions (or neutrals) which then produce cascade emission lines. Observational evidence of CX emission has been obtained from the optical band in many SNRs for over 30 years [9, 19]. However, the study of CX-induced X-ray emission in SNRs is still limited. Possible evidence has been found for a number of SNRs, including Galactic remnants Cygnus Loop [42, 80, 99], Puppis A [41], and G296.1-0.5 [94], SMC remnant 1E0102.2-7219 [76], as well as LMC remnants N132D [93] and J0453.6-6829 [46]. These studies are mostly based on investigations into the O VII triplets: the CX emission could be indicated by an unusually high G ratio. However, the precise measurement of G ratios could still be challenging with current X-ray instruments. CCD cameras are not able to resolve the He-like triplets, which are shown as one single line in the spectrum. Thereby one can only roughly estimate the G ratio based on the line centroid

energy, which may lead to large uncertainties. In addition, CCD observations may be contaminated by the emission from solar wind charge exchange (SWCX). Grating instruments can help to resolve the triplets and to improve the constraint on G ratios, but the energy resolution may still be affected by the angular size of the source (morphological broadening). On the other hand, an enhanced G ratio is not necessarily originated from CX, it can also be induced by other mechanisms such as resonant scattering and inner-shell ionization. One possible way to distinguish CX from other mechanisms is to look for enhanced high-level excitation lines (e.g., enhanced Lyγ/Lyβ line ratios), which is another prominent and unique feature of CX emission. However, these lines are usually too weak to be detected or blended with other emission lines. Taking together the spatial resolving ability, the high energy resolution, and the large effective area, HUBS provides us with an unprecedented opportunity to study the CX phenomenon in SNRs.

Due to the rather low density, the hot X-ray plasma in SNRs can be safely assumed as optically thin in most cases. However, for some emission lines with large transition oscillator strengths, the resonant scattering (RS) effect may not be ignored when the remnant contains a large column density. The optical depth at the line centroid can be estimated following [34]:

$$\tau = \frac{4.24 \times 10^{26} f N_{\rm H} \left(n_{\rm i}/n_{\rm z}\right) \left(n_{\rm z}/n_{\rm H}\right) \left(M/T_{\rm keV}\right)^{1/2}}{E_{\rm eV} \left(1 + 0.0522 M v_{100}^2/T_{\rm keV}\right)^{1/2}} \tag{1}$$

where f is the oscillator strength of the line, $E_{\rm eV}$ the line centroid energy in eV, $N_{\rm H}$ the hydrogen column density in cm^{-2}, $n_{\rm i}$ the ion density, $n_{\rm z}$ the element density, M the atomic weight, $T_{\rm keV}$ the plasma temperature in keV, and v_{100} the turbulence velocity in 100 km s^{-1}. Taking the O VII resonant line ($f \sim 0.72$) as an example, in a dense remnant like SN 1987A ($n_{\rm e} \sim 2400\,{\rm cm}^{-3}$ [92]) or a large remnant like Cygnus Loop (diameter of $\sim 2^\circ.8$ at a distance of ~ 540 pc [48, 5]), the column density may go to $N_{\rm H} \gtrsim 10^{20}\,{\rm cm}^{-2}$, resulting in an optical depth $\tau \sim 1$. The RS process will scatter the incident photon into another random direction. For a non-uniform distribution of the plasma or an asymmetric remnant, it will then change the line flux and modify the surface brightness distribution. Therefore, similar to CX, RS may also be indicated by an enhanced G ratio — in this case, it is due to the reduced resonant line flux rather than the enhanced forbidden line flux. The RS effect in X-rays has been extensively studied in diffuse hot plasma of massive elliptical galaxies, galactic bulges, and clusters of galaxies [108, 8, 26]. The current study on the X-ray RS effect in SNRs is still quite limited. One possible observational evidence comes from the LMC remnant N49, for which people find enhanced O VII G ratio as well as O VIII Lyβ/α and Fe XVII $(3s\text{–}2p)/(3d\text{-}2p)$ ratios, indicating RS effect on several resonant lines [1]. HUBS will be capable of resolving all of the bright resonant emission lines lying in the 0.1–2 keV band. Taking advantage of its spatially-resolved high energy resolution and the large field of view, we will be able to map out the surface brightness distributions of individual emission lines for the whole remnant, which has never been done before and will certainly improve our insight into the RS effect in SNRs.

2.3.1 Cygnus Loop

The Cygnus Loop could be one of the most suitable sources for studying the CX and RS effects in SNRs. It is a nearby SNR at a distance of 540 pc [5], and is thought to be from a Type II SN that exploded around 10^4 years ago [98, 39]. It is a prototypical shell-type SNR with a limb-brightened morphology in both X-ray and radio bands. The X-ray emission along the rim mainly raises from the shocked ISM, showing a relatively low temperature ($kT_{\rm e} \sim 0.2$ keV) and sub-solar abundances [98]. It is also at the rim where CX and RS could be taking place. The CX process represents a neutral atom (mostly hydrogen) hit with a highly ionized ion (e.g., O VII, O VIII) at a high relative speed and exchange one electron, and this is exactly what could happen just behind the forward shock front in SNRs — the up-stream neutral hydrogen atoms may cross the shock and mix with the down-stream ions. On the other hand, the column density of specific ion species (such as O VII) at the rim could be high enough to have a large optical depth $\tau \sim 1$ for RS, which may modify the line flux and the line profile. Based on Suzaku observations, people have found enhanced high-level transition (e.g., Heγ) emission from O VII and redshifted O VII Heα triplets at several positions along the rim of Cygnus Loop, which provide evidence for CX processes [42, 80]. More detailed high-resolution spectroscopy study using RGS observations also reveals an unusually high forbidden-to-resonance O VII line ratio at a bright knot near the southwestern rim of Cygnus Loop, which could be due to the CX [99]. However, the effect of RS cannot be ruled out for these features mentioned above.

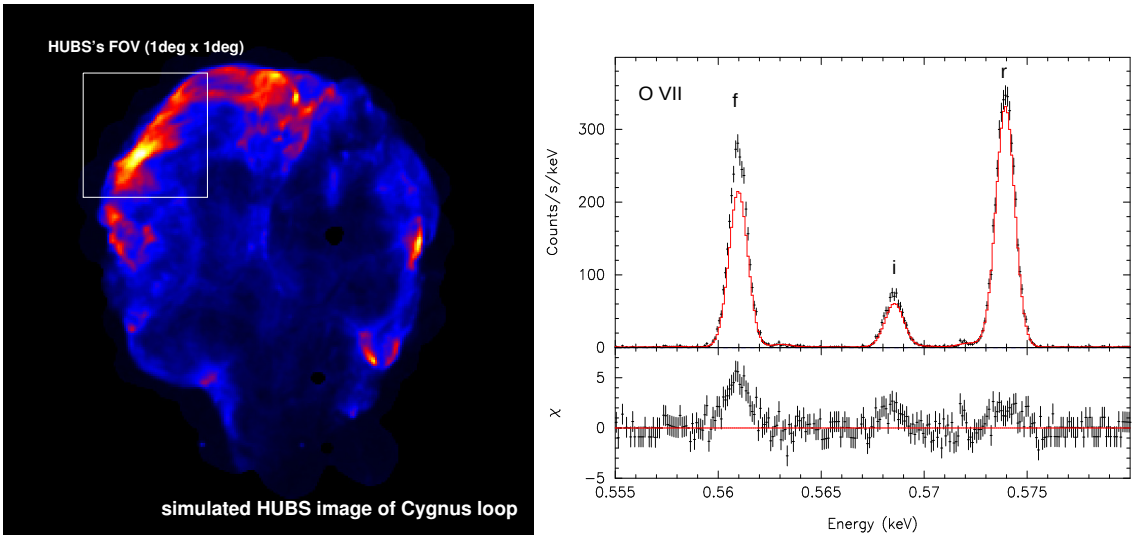

Figure 6: Left: Simulated HUBS image of Cygnus Loop, with the white box denotes the HUBS's field of view ($\sim 1^\circ \times 1^\circ$). Right: Simulated 20 ks HUBS spectrum of the OVII triplet from $2' \times 2'$ region with CX process (black data points). The red solid line shows a pure under-ionized plasma model, which underestimates the forbidden-to-resonance line ratio.

HUBS may help us further clarify the roles CX and RS play in the case of Cygnus Loop. The right panel of Figure 6 shows a simulated O VII triplet in a $2' \times 2'$ region in the SNR northeast. With a CX component implanted, the forbidden-to-resonance line ratio is expected to be enhanced compared to a pure under-ionized plasma model (e.g., *neij* in SPEX). The figure shows that a 20 ks HUBS observation will allow us to resolve the triplet and probe the CX process using line ratios.

2.4 Probe the kinematics of the shocked ejecta/CSM and resolve the collisionless shock heating mechanism

The kinematics of SNR represents the spatial and velocity distribution of the shocked ejecta and CSM, which provides great information of the explosion mechanism, the progenitor system, and the remnant evolution.

One of the most important features of SN explosion concerns the structure of the ejecta, especially, whether it is symmetrically distributed or not — and if not, how asymmetric it is. It has been suggested that the overall distribution of the ejecta in Type Ia remnants is more symmetric, while in core-collapse remnants it could be more asymmetric [51, 52]. An example of the core-collapse SNRs is Cas A. Based on the kinematic studies in different energy bands, people have been able to construct the three-dimensional distribution of the ejecta in Cas A [61, 62], which shows great asymmetry with multiple rings, bubbles, and jets. All of these structures may be formed in the SN explosion and the shock breakout process, indicating a highly asymmetric explosion mechanism. On the other hand, a comparison between the core-collapse SNR asymmetries with the neutron star (NS) kick indicates that the bulk ejecta material is distributed opposite to the NS kick direction, which supports the theory that NS kicks are caused by ejecta asymmetries but not by anisotropic neutrino emission [28]. Type Ia remnants seem to be more spherically symmetric, which is likely because they typically evolve in a relatively isotropic and uniform environment. However, there are still some exceptions, such like Kepler with two "ears" and 3C 397 with a box-like shape. That may indicate the asymmetric explosion mechanisms of Type Ia SNe.

The kinematic studies can also provide indications to the remnant evolution properties. For example, measuring ejecta distribution may help to estimate the location of the reverse shock (RS). When using ejecta abundances to infer the SN type, how much ejecta has been shocked can always be a problem — since only the ejecta that already shocked by the RS emits X-rays. That makes estimating the location of the RS very important. Many attempts have been make on determining the RS locations in SNRs. For example, based on Chandra LETG/HETG observations, people measured the

radial velocity of the ejecta knots in G292.0+1.8, together with the projected location of these ejecta knots, it indicates an RS position very close to the outer boundary of the central pulsar wind nebula (PWN), which leads to the possibility of the RS-PWN interaction [3]. Similar method has also been used for Tycho, where the RS is suggested to be at $\sim 2'.0$–$2'.6$ from the remnant center [64]. Other applications of kinematic studies on SNRs include estimating the expansion parameter, which provides clues to the surrounding environment of the remnant.

The high energy resolution of HUBS is especially good for measuring the Doppler shifts of emission lines, and thus for determining the radial velocity of the remnant or the ejecta/CSM clumps. Therefore, it can help to improve our understanding on the SNR kinematics. Combine with the proper motion observations by Chandra and other instruments, HUBS will also help to construct the three-dimensional model for more remnants.

On the other hand, HUBS is also adequate for studying the line broadening, which can be used to indicate the kinematic properties of the SNRs as well. However, things could be more complicated since the line broadening may be caused by many other mechanisms such as the instrumental broadening and the thermal broadening. But in that sense, it could be good for us since it provides also information on these mechanisms. For example, the line broadening may used to estimate the post-shock ion temperatures in SNRs. One of the major topics in SNR science is the shock physics. The shocks in SNRs are typically "collisionless", where the thickness of their jump region is much shorter than the collisional mean free path of the particles. Then, how the particles be heated, especially the dependence of the post-shock temperature on the particle mass is still under debate. The thermal broadening of the emission lines provides a direct way to derive the post-shock ion temperatures. Based on RGS observations, the broadened O lines give an ion temperature $\sim 500\,\mathrm{keV}$ at the rim of SN 1006 [104]. Using HETG data, people found the ion-to-proton temperature ratios are significantly greater than one in SN 1987A [60]. HUBS may expand our knowledge on the collisionless shock heating process.

2.4.1 Kepler's SNR

Kepler's SNR is an ideal target for HUBS in studying the plasma kinematics. Both of its location, its historical light curve, and its Fe-rich ejecta indicate Kepler originated from a Type Ia explosion. However, the remnant shows also significant CSM features. The bulk velocity against the galactic plane and the bow-shock-like structure of the shocked CSM suggest that the progenitor of Kepler was a runaway system. The mass and abundances of the CSM indicate a single-degenerate progenitor system where the donor star is likely a $\sim 4\,M_\odot$ AGB star. But as mentioned in Section 2.1.1, there are still problems about the progenitor system and the explosion mechanism of Kepler. The kinematic information of the shocked ejecta and CSM may provide further clues to these questions.

Proper motion measurements have been performed at multiple energy bands for Kepler. In X-rays, with the help of the high angular resolution of Chandra, people have measured the proper motions of the forward shock along the rims of the remnant [101, 38]. There are two major indications based on proper motion studies: one is the distance to the remnant, which is an essential scaling factor in determining many other parameters; and the other one is the expansion parameter which is deeply related to the remnant evolution and its surrounding environment. The Chandra proper motion measurements indicate a distance to Kepler as $3.3^{+1.6}_{-0.4}\,\mathrm{kpc}$ [38], and the expansion parameter as $r \propto t^{0.5}$ on average but $r \propto t^{0.35}$ at the bright northwestern rim [101, 38].

On the other hand, constraints on the radial velocity rely on the Doppler shift measurements of emission lines. In X-ray band, radial velocities have been measured using HETG for several bright knots in Kepler [63] and using RGS for different parts of the remnant [36]. HUBS can greatly improve the accuracy and the coverage of line shift measurements. In Figure 7, we present simulated 100 ks HUBS central array observations of several major emission lines from Kepler, including Fe XVII+O Lyγ, Ne Heα, and Mg Heα. The relatively narrow, red-shifted CSM component and the broad, blue-shifted ejecta component can be well distinguished in HUBS spectrum. One can then measure the radial velocity and the Doppler broadening individually for the CSM and the ejecta with an accuracy of 10–100 $\mathrm{km\,s^{-1}}$ (see also the discussion in next Section on SN 1987A). A spatially-resolved accurate measure of the radial velocity based on HUBS, together with the previously obtained proper motions, can be used to construct the three-dimensional kinematic map of Kepler, as previously done for Cas A [61, 62], which could be a great leap toward the understanding of its explosion nature.

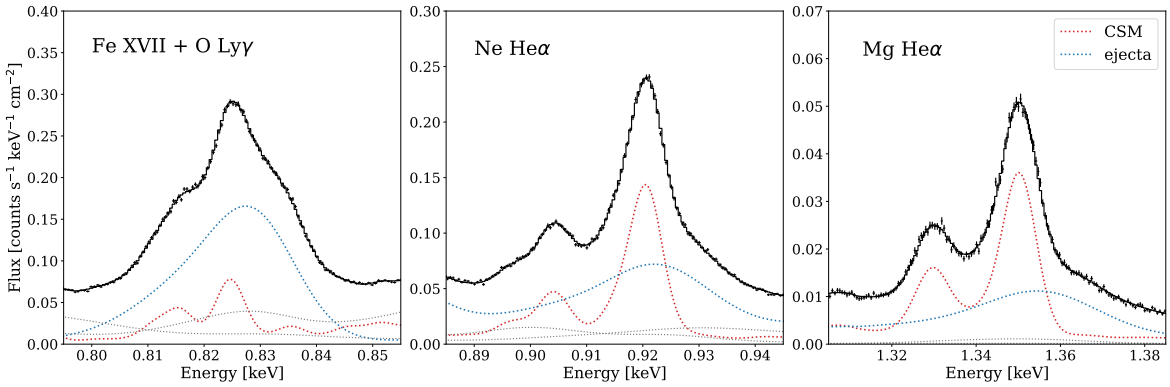

Figure 7: Simulated 100 ks HUBS central array observations of several major emission lines from Kepler's SNR. The narrow ($\sim$ 800 km s^{-1}), redshifted CSM component (red dotted lines) and the broad ($\sim$ 2700 km s^{-1}), blueshifted ejecta component (blue dotted lines) can be well distinguished by HUBS.

2.4.2 SN 1987A

SN 1987A was a Type II SN detected on 1987 February 23 in the Large Magellanic Cloud (LMC). It is the nearest SN observed since Kepler's SN of 1604, thus provides us with a unique opportunity to study in detail the onset of SNR formation and subsequent evolution. SN 1987A is also an ideal laboratory for the studies of many astrophysical processes, including the gas kinematics and the collisionless shock heating mechanism.

The X-ray emission of SN 1987A mainly comes from the dense CSM torus — the so-called "equatorial ring", and the spectrum is dominated by various metal lines from the thermal-emitting gas. The line broadening effect has been investigated with the Chandra LETG/HETG and XMM-Newton RGS observations, which detected significant broadening for most of the bright lines, and the obtained line widths convert to a bulk gas velocity $\sim$ 200–1000 km s^{-1} [114, 88]. A recent study based on both the observations and the three-dimensional hydrodynamic simulation shows that the line broadening in SN 1987A could be also due to the thermal effect, which can be used to constrain the post-shock ion temperatures [60]. They found the post-shock ion-to-proton temperature ratios to be significantly greater than one and increasing linearly with the ion mass, providing new insight to the collisionless shock heating mechanism.

With a larger effective area and an even better energy resolution than the existing grating instruments such like LETG/HETG and RGS, HUBS is especially adequate for measuring the line shift and line width. The upper penal of Figure 8 presents a simulated 100 ks HUBS central array spectrum of SN 1987A, which shows the well resolved line features. With the help of HUBS, we can measure the line shifts and line widths not only for those most luminous, but also for the relatively weak lines. As illustrated by the lower penals in Figure 8, HUBS provides tight constraints on the centroid energies and the widths for over 30 emission lines, with an uncertainty down to $\sim$ 10 km s^{-1} for those most luminous lines and $\sim$ 100 km s^{-1} even for the weakest lines. This will certainly help to improve our understanding on the CSM/shock structure of SN 1987A, and extent our study into more metal species.

Other potential HUBS targets on this topic include SN 1006, Cas A, SNR 0519−69.0, etc. High radial velocity ejecta clumps with $\pm$4000–6000 km s^{-1} have been detected at the central region of SN 1006. Meanwhile, at the rim of SN 1006 people have found broadened O lines which indicate an ion temperature $\sim$ 500 keV [104]. Cas A is one of the few SNRs whose three-dimensional ejecta structure has been constructed [61, 62]. SNR 0519−69.0 is the second brightest LMC Type Ia remnant seen in X-rays. Optical observations indicate a forward shock velocity $\sim$ 2600–4500 km s^{-1} [20], and line broadening has also been detected in X-ray band with [75]. HUBS may help to further investigate the kinematic properties of these remnants.

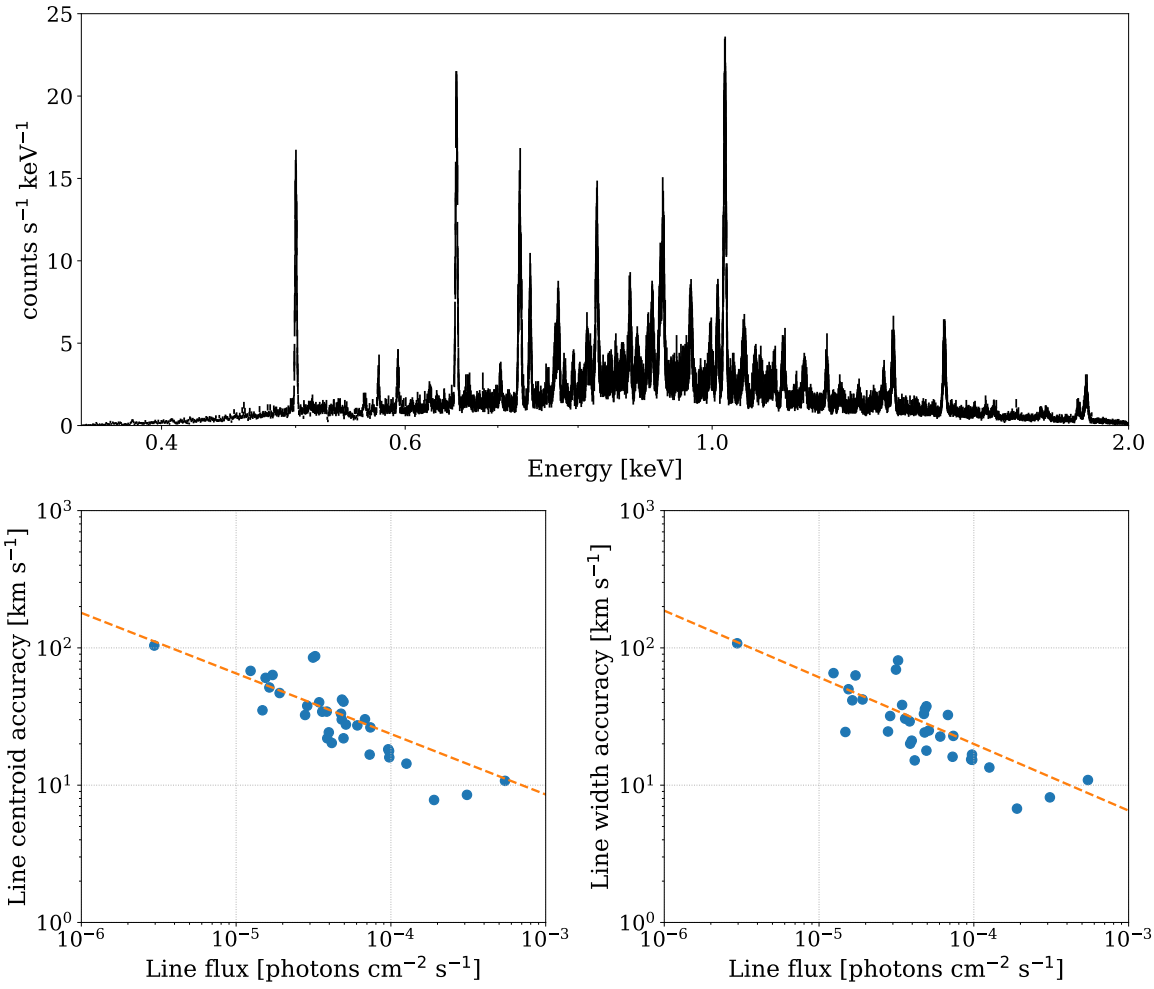

Figure 8: Upper panel: simulated 100 ks HUBS central array spectrum of SN 1987A (based on the latest XMM-Newton RGS observation). Lower left panel: 1-σ uncertainties of the line centroid energy measurements based on the simulated HUBS observation. Lower right panel: 1-σ uncertainties of the line width measurements.

2.5 Construct high resolution X-ray spectroscopy sample of Magellanic Cloud SNRs

More than 300 Galactic SNRs has been discovered so far, and over half of them exhibit X-ray emission. However, based on the SN rate and the lifespan of the remnant, there is expected to be more than 1,000 SNRs in our galaxy. One possible reason why there are still many SNRs missing could be that they are subjected to heavy absorption along the Galactic plane. Therefore, a complete sample of the SNRs in a galaxy can be better studied in those nearby galaxies rather than in our Milky Way. Another advantage for nearby galaxies is that the distance to them are well constrained, and we can assume all the SNRs in one galaxy to be at a similar distance. Compare to those remnants in the Galaxy, this may greatly reduce the distance uncertainties.

The Large Magellanic Cloud (LMC) and the Small Magellanic Cloud (SMC) are two neighbour galaxies of Milky Way, which provide ideal laboratories for the study of the SNR populations. The X-ray survey of LMC and SMC has been done by many telescopes and the X-ray SNR populations have been studied recently based on XMM-Newton observations [54, 55]. The X-ray luminosity and angular size as been measured for all these remnants. And for those X-ray-bright remnants, the CCD spectra have been fitted using collisional ionization plasma models, from which the temperatures, ionization parameters, and the metal abundances of the shock-heated gas have been constrained. Based on the spectral analysis results, the core-collapse SNR fractions are estimated to be ~ 0.57 in LMC and ~ 0.62–0.92 in SMC. The abundances of O, Ne, Mg, Si, and Fe in the hot phase of ISM are found to be ~ 0.2–0.5 in LMC and ~ 0.1–0.2 in SMC [54, 55], which fills the gap of the abundances of intermediate-mass elements that supplements the optical/UV studies [29].

The high energy resolution as well as the large field of view makes HUBS a perfect telescope for high resolution X-ray spectroscopic survey, and its modest angular resolution ($\sim 1'$?) allows us to distinguish the emission of the shocked ISM from that of the shocked ejecta. With the help of HUBS, we will be able to construct the first high resolution X-ray spectroscopy sample of the Magellanic Cloud SNRs, and carry out the spectral diagnosis beyond the CIE assumption. This analysis may provide much better constraint on the chemical and thermal properties of the shocked gas, give us deeper insight on the hot phase ISM in LMC and SMC.

3 Compact Objects

Contributors: Zhaosheng Li, Xiaojie Xu, Song Wang, Heng Xu, Weiyang Wang, Shi Dai, Xiaoyu Lei, Kejia Li, Helei Liu, Jiguang Lu, Lijing Shao, Lian Tao, Hao Tong, Hongguang Wang, Zhongxiang Wang, Yi Xing, Renxin Xu, Liyun Zhang, Enping Zhou, Jianeng Zhou, Weiwei Zhu

As the fundamental units of galaxies, stars play a key role in the recycling of matter. X-ray observations associated with stars not only deepen understanding of a wealth of astronomical phenomena, but also contribute to the understanding of extreme physical processes.

Several crucial questions have to be answered with HUBS: 1) Can we detect spectral features on the neutron star (NS) surface or the sourrounding accretion disk to constrain the NS equation of state? 2) How does the hot plasma near the WD surface in the accretion column/boundary layer cool and how are the emitted X-ray photons absorbed by the accreted matter? 3) How to understand the X-ray flare mechanism and coronal heating process?

HUBS, with its large area and high spectral resolution, will clarify these unanswered questions about neutron stars, white dwarfs and active stars.

3.1 Neutron Stars

NS formed by supernova explosions are the most compact objects in the universe. The equation of state for cold and dense matter is still inconclusive with respect to the understanding of the non-perturbative nature of the fundamental interactions between quarks [47]. The equation of state of NS and strangeon star predict different mass-radius relations [87, 107]. The accurate measurements of NS mass and radius could put stringent constraints on the equation of state [71]. Mass measurements of massive NS, $M > 2M_\odot$, have been already excluded a number of equations of state that predict the maximum mass smaller than $2M_\odot$ [15]. Although a number of masses of NSs in compact binaries have

been measured from radio observations with high precision, radius measurements are much difficult to achieve with a comparable precision.

Usually, NS mass and radius can be measured from type I X-ray bursts occurred in NS low-mass X-ray binaries (LMXBs), pulse profile modelling of X-ray pulsars and so on. NS LMXBs are composed of NS and a main sequence donor orbiting each other. The masses of the NS and its companion can be determined by kinetic methods, with the orbital motion of the star in the NS LMXBs causing its spectral lines to undergo periodic redshifts and blue shifts due to the Doppler effect. The optical and/or near-infrared (NIR) spectroscopic observations can determine the mass function (stellar radial velocity profile) of the star. Over the past decades, optical/NIR observations have shown that this method has the potential to constrain the compact object mass of LMXBs. However, there are also some shortcomings, mainly in that (1) this method requires a relatively bright optical/infrared flux of stars in LMXBs with strong absorption or emission lines, which is difficult with current optical/NIR telescopes for optically faint LMXBs; (2) This method can only measure the stellar mass function, but not the dense stars. If we can use an X-ray telescope with high energy resolution and large effective area, we will be able to measure the velocity profile of dense stars and obtain the mass function of compact stars, which can be combined with optical/NIR observations to measure the binary mass ratio. The masses of compact stars can be constrained more precisely if the stellar masses can be determined from optical observations. This has important implications for the mass spectrum of black holes and neutron stars, and for the solution of the "mass gap" problem. Even if the stellar masses cannot be determined, the mass ratio of the two objects, combined with other measurements, can be used to constrain the binary masses as well.

We carry out a series of simulation by using the ancillary response file, hubs_cc_s_v20181102.arf, and the redistribution matrix file, hubs_cc_s_v20181109.rmf. The data are produced by using the command fakeit in Xspec 12.13.0c. Since the background file is unavailable, the simulations do not take the background into account, which can be updated in future.

3.1.1 The eclipsing low-mass X-ray binaries

Eclipsing low-mass X-ray binaries are high inclination systems with the inclination angle larger than 75°. Zhang et al. [113] suggested that absorption lines from accretion disk winds are redshifted or blueshifted due to the Doppler effect of orbital motion. These spectral features are produced in the vicinity of compact objects and trace their motion, which can constrain the mass of compact objects in LMXBs. This approach was subsequently applied to the eclipsing NS LMXB MXB 1659–298, but the uncertainties of the measured radial velocities are large because the energy resolution of Chandra and NuSTAR is not high enough [74]. In general, the maximum radial velocity of compact objects in X-ray binaries is in the order of 100 km/s, which causes a spectral shift of order 10^{-4}. Therefore a high energy resolution of the detector is required. The energy resolution of HUBS has the possibility to measure the Doppler shift of the spectral lines with high precision.

We perform the HUBS simulations for MXB 1659–29. This source is an eclipsing NS LMXB, which has an orbit period of 7.1 hr [12]. Based on the results from [74], we adopt the continuum spectrum which has an absorbed flux of 5×10^{-10} erg cm^{-2} s^{-1} in the energy range of 0.1–2 keV and a blackbody temperature of 3 keV. The Mg XIII Lyα absorption line centering at 1.472 keV, which is covered by HUBS, is also added. The exposures of 1 ks, 10 ks and 100 ks are simulated for each observation. For the whole orbit period, we carry out 12 observations with uniform separations. In order to measure the radial velocities at different orbital phases, we focus on the Mg XIII Lyα line and determine its shift. The left panel in Figure 9 shows the spectral lines at the orbital phases of 0 and 0.75, in blue and orange, respectively. The vertical dotted line is the central energy of the spectral line at that phase. The right panel in Figure 9 presents the simulation data with errors and the solid lines for the best fitting model. For the case of 10 ks exposure, the maximum radial velocity is constrained at 89.84 ± 2.73 km/s, and the mass function of NS can be achieved with $f = 0.022 \pm 0.002 M_{\odot}$. Besides MXB 1659–298, there are many eclipsing binaries can perform such studies, such as, XB 1832–330, MXB 1728–34, GX 13+1, 4U 1626–67, 4U 1538–52, 4U 1916–05 and 2S 0921–630.

3.1.2 Symbiotic X-ray Binaries

Symbiotic X-ray binaries (SXBs) are a special subclass of NS LMXBs, which host a neutron star accreting matter from a M-type giant companion, rather than a dwarf. Usually, the orbital periods

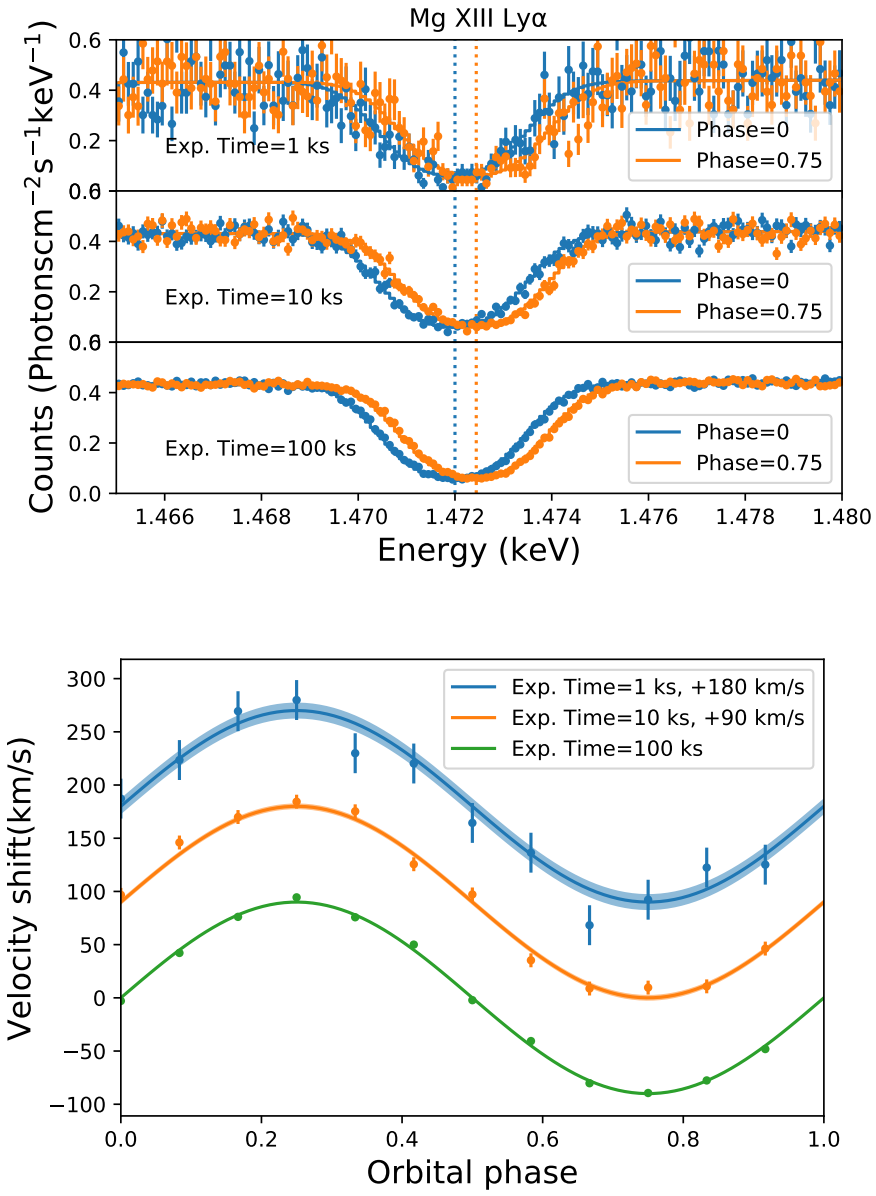

Figure 9: Top panel, from top to bottom, the spectral simulation of MXB 1659–298 center around the Mg XIII Lyα line with exposure times of 1 ks, 10 ks, and 100 ks, respectively. The blue vertical dotted line is the spectral line Mg XIII Lyα in the rest frame, and the orange vertical dotted line is blueshifted as a factor of 3×10^{-4}. Bottom panel, the radial velocities and uncertainties observed at different orbit phases.

of SXBs and the spin periods of the neutron star are both long. Among them, 4U 1954+31 is the longest accreting neutron star with a spin period of about 18300 seconds (Masetti et al. 2006). Why do neutron stars in SXBs have such long spin periods? The standard disk accretion model does not explain it yet. At present, the rotation periods of nearly half of the SXBs have yet to be determined, and it remains to be confirmed whether they are all longer. In addition, we also need to study the spin period evolution of SXB due to accretion, to test the recycling scenario of the traditional millisecond pulsar (Alpar et al. 1982). The possible presence of ultra low-mass neutron stars in such systems, if confirmed, would pose a great challenge to the equation of state of neutron stars (Xu 2004). On the other hand, if we can measure the masses of neutron stars in these systems, we will be able to refine the neutron star mass spectrum. The vast majority of SXBs do not have measured orbital periods, and if we are able to measure them well, we will also be able to further understand the evolution of LMXBs.

The SXB 4U 1700+24 has a red giant donor. Its X-ray emission is dominated by wind accretion. In the X-ray spectrum of 4U 1700+24, the O VIII (hydrogen-like Ly-α) emission line is observed with a central energy of 0.65 keV [69]. The emission line is corresponding to a gravitational redshift of 0.009, suggesting that 4U 1700+24 is an ultra low-mass neutron star candidate, which has to be verified by HUBS observations [109].

The continuum spectrum of 4U 1700+24 consists of a blackbody, a Gaussian and a Compton scattering component (Tiengo et al. 2005). The blackbody has a temperature of 1.4 keV and the Comptonization of the photons leads to an increase in the flux of high-energy photons, which results in a strong flux in the 0.1–2 keV band. To simulate the series of Ly-α lines, we added three Gaussian emission lines whose energies correspond to the energies of each of the Ly-α lines, each with a width of 20 eV. Since the 652.8 eV line has been observed in XMM-Newton, we assume that the intensity of the remaining lines is half of the 652.8 eV line intensity. The exposure time was 10 ks, and the spectrum simulation are shown in Fig. 10.

3.1.3 Type I X-ray bursts

The unstable thermonuclear burning of the helium and mixed of hydrogen and helium, also known as type I X-ray burst, usually has the duration of $\sim 10 - 100$ s with a typical energy release of 10^{39} erg, recurs from few hours to days, and ignites at a column depth of $\sim 10^8$ g cm^{-2} [17]. In a more rare case, superbursts, which are believed due to unstable burning of carbon, have been identified from the total energy release of $\sim 10^{42}$ erg and the duration of $> 10^3$ s [14]. Cottam et al. [13] reported the identification of absorption lines by stacking of XMM-Newton spectra over dozens of type I X-ray bursts from NS LMXB EXO 0748–676, which they claimed were gravitational redshifted Fe and O lines from the stellar surface. However, the spectral lines have not been confirmed by the following observations (Cottam et al. 2008). This particular source is now believed to be rotating rapidly with frequency of 552 Hz from its burst oscillation [18], which makes it challenging to explain the relatively narrow spectral features reported in [13]. in't Zand et al. [31] also reported the none detection of spectral lines in Rapid Burster from Chandra/HETG observations. Rauch et al. [77] calculated the possible spectral lines in the soft X-ray band, i.e., Fe and O, that can be generated during type I X-ray bursts. Why the spectral lines during type I X-ray bursts have not been detected by XMM-Newton or Chandra? The spectra could evolve quickly in a normal type I X-ray burst, due to the photosphere expandsion and contraction on NS surface. By stacking the spectra in the raise and decay stages separately from dozens of type I X-ray bursts would not increase the signal-to-noise ratio of spectral lines. Another possibility is the effective ares of the high energy resolution detectors on board of XMM-Newton and Chandra are not too large.

The characteristic spectral lines of Fe XXVI, Fe XXV, and O VIII are in the 0.1-2 keV energy band and can be observed by HUBS. In order to confirm the possible appearance of spectral features in the EXO 0748-676 during type I X-ray bursts, we assume that the continuum spectrum is a blackbody emission of $kT \sim 1.8$ keV, which is close to the Eddington luminosity, and the absorption line (FeXXVI) has an central energy of 0.954 keV and a width of 20 eV. We chose an exposure time of 100 s. The simulated X-ray burst energy spectrum is shown in Fig. 11. It is worth noting that the 100 s exposure is usually too long for a single bursrt, since its spectra usually evolve rapidly as mentioned above. The energy of spectral line may change during a normal type I X-ray burst. The spectra can be combined at the same stage from burst samples, such as the peak and the touchdown moment. Moreover, from a single superburst, we can obtain long exposure spectra with sufficient X-ray photons to produce

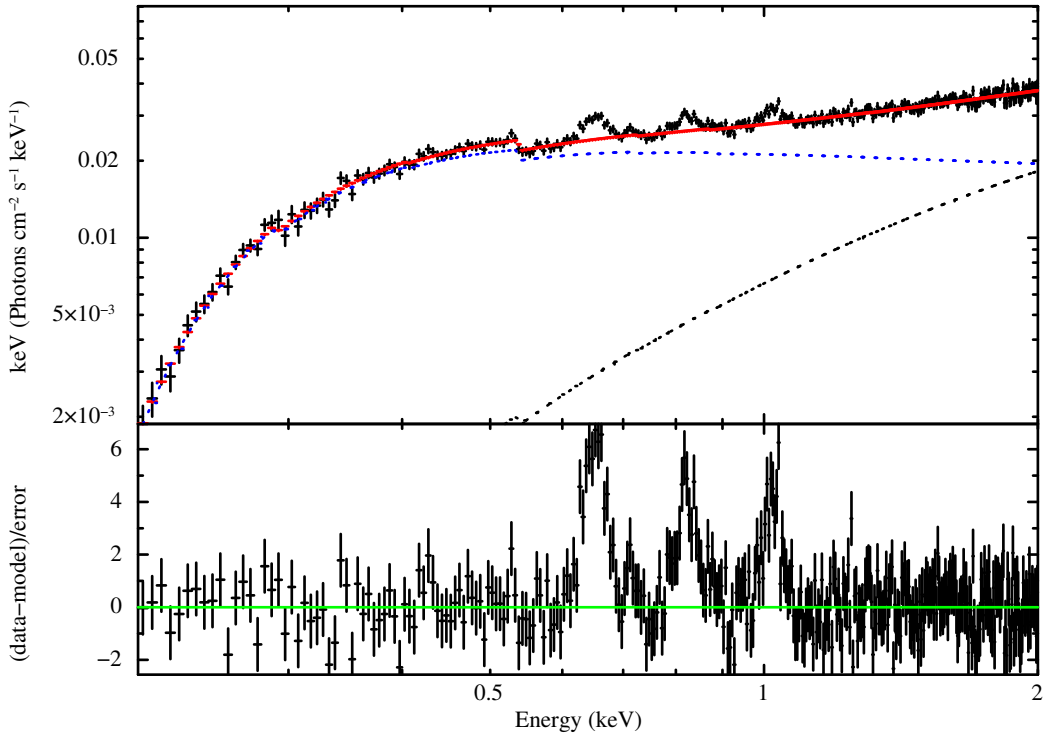

Figure 10: The simulated X-ray burst spectrum of 4U 1700+24. The continuum model is `phabs*(bbodyrad+compST+gaussian+gaussian+gaussian)`. The exposure time is 10 ks. The central energies of three emission lines are 0.65 keV, 0.82 keV and 1.02 keV, respectively. All the line width are 0.02 keV. The normalization of the gaussian compontents are 5×10^{-4} photons cm^{-2} s^{-1} for the 0.65 keV line and 2.5×10^{-4} photons cm^{-2} s^{-1} for other two lines. The red line fits the spectrum by a blackbody plus compST model.

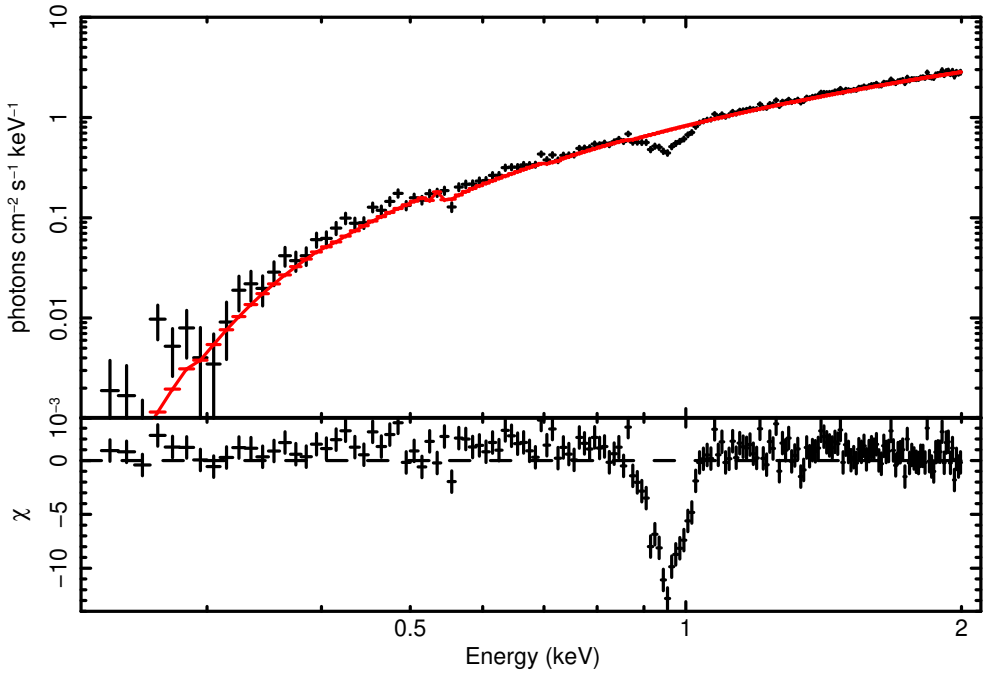

Figure 11: The simulated X-ray burst spectrum of EXO 0748–676. The continuum spectrum is a blackbody with temperature of 1.8 keV. The exposure time is 100 s. We assume the Eddington limit is reached. We add an absorption line at 0.954 keV and width of 0.04 keV. The red line fits the spectrum by a blackbody model. The absorption line is clearly shown in the residual.

significant spectral lines.

The X-ray dimmed isolated neutron stars The X-ray dimmed isolated neutron stars (XDINSs) mainly emit blackbody spectra in X-ray bands, and show optical/ultraviolet (UV) excesses [24]. All the seven known XDINSs were found by soft X-ray instruments. RX J1856–3754 is the brightest and closest neutron star. Chandra observations showed that RX J1856–3754 had an almost blackbody spectrum in the soft X-ray band, with no emission or absorption lines [7]. Absorption lines may be present in other XDINSs, which need to be confirmed. It is generally believed that the soft X-ray thermal spectrum of XDINS comes from the surface of the star. The absorption lines in the XDINS spectrum are produced in the magnetic environment of the neutron star. Moreover, the structure of the absorption lines is related to the stellar surface properties. Wang et al. (2017) [105] proposed that the accretion of the interstellar medium to form the atmosphere of a strangeon star, and that the accreted atmosphere may produce absorption features. The temperature and radius of the continuum spectrum depend on the equation of state of the dense star (see [27] for neutron stars; [105] for strangeon stars). The mechanisms of absorption line generation are related to the equation of state of compact object, such as the equally spaced cyclotron absorption lines of electrons or protons in a magnetic field, collective oscillations of electrons on the strangeon star surface, etc. The mechanism of absorption line generation can be inferred from the energies of multiple spectral lines. Therefore, XDINS is an excellent target to study the surface properties and the equation of state of neutron stars.

We choose the input model `phabs*bbodyrad*gabs` for the XDINS RX J0806.4–4123. The exposure time is 70 ks. The blackbody spectrum of RX J0806.4–4123 has a temperature of 0.1 keV, a normalization of 100, and a hydrogen column density of 1×10^{20} cm^{-2} (see Kaplan et al. 2011). To describe the absorption line structure, we added a Gaussian absorption component with an energy of 460 eV and width of 40 eV (see Haberl et al. 2004). The simulated data and the blackbody fit are shown in Fig. 12.

Besides measuring the NS mass and radius, HUBS can also study the magnetic field of anomalous X-ray pulsars (AXPs) and soft-γ-ray repeaters (SGRs). AXPs and SGRs are slowly rotating, isolated and ultramagnetized neutron stars [35, 59]. Their X-ray activities, short bursts and outbursts, are powered by magnetic energy. During outbursts, the X-ray spectra of AXPs and SGRs may appear absorption line, which is interpreted as a proton cyclotron feature. HUBS could resolve the absorption features in 0.1–2 keV from AXPs and SGRS, and measure the magnetic field (see e.g., [96]).

3.1.4 Cataclysmic Variables

Cataclysmic variables (CVs) are binaries consisting a white dwarf (WD) and a late type main sequence or sub-giant star. CVs are the most populated binaries consisting a compact star and their spatial density can reach up to 10^{-6} to 10^{-5} pc^{-3} in the solar neighborhood [84]. The WD in a CV accretes matter from its companion and emit mostly in UV and X-ray energy range. CVs are not only laboratories of stellar evolution theory, but also related to other important astrophysical questions. For example, CVs collectively contribute up to 80% of the Galactic Diffuse X-ray Background (GDXE). What's more, CVs are closely related to the progenitor of type Ia supernovae since the latter are supposed to binaries harboring one or two WDs.

X-ray observations provides unique information to understand the accretion and emission process of CVs. the X-ray luminosity of CVs can reach 10^{33-34} erg s^{-1}, high enough to study the structure of the X-ray emitting region through X-ray spectroscopy. For example, the hard X-ray (around 2 to 50 keV) spectra of CVs have been well described by multi-temperature thermal plasma model (mkcflow), and are used to constrain the maximum emission temperature and the mass of the WD. In contrast, the soft (0.1-2 keV) X-ray spectra of CVs are less well understood, and the usually characterization (the same mkcflow emission partially covered by the accreted matter) failed to explain the He-like and H-like lines from different elements (e.g., C, N, O) [66, 72]. Until now, there are only 15 CVs with high resolution X-ray spectra at present, and about half them are not well explained. Since the soft X-ray are supposed to be originated from the region fairly close to the surface of the WD, the fail of a widely-accepted model in this energy range leads to the lack of understanding of the accretion process near the WD itself.

HUBS provides a unique opportunity to explore the details of the emission region in CVs. The high-resolution spectra would certainly allow detailed investigation on the distribution of the differential emission measure (deM) and the metallicity on a large sample of CVs. Combined with hard X-ray

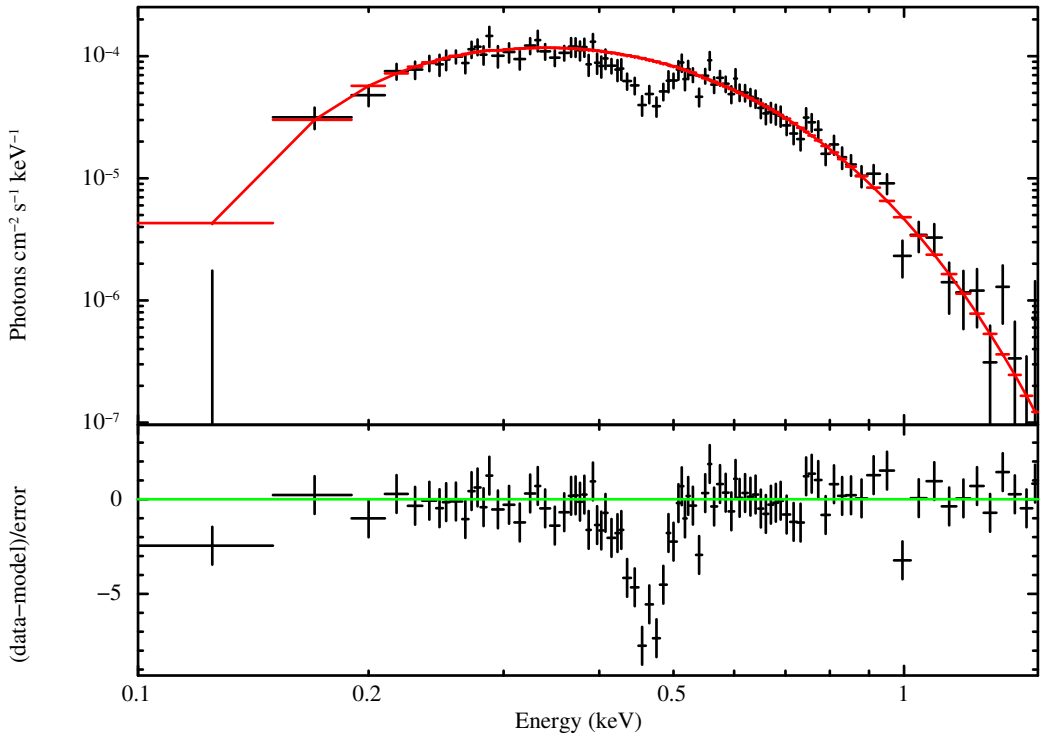

Figure 12: The simulated thermal spectrum of the XDINS RX J0806.4–4123. The continuum spectrum is a blackbody with temperature of 0.1 keV. The blackbody normalization is 100. The exposure time is 100 ks. We add an absorption line at 0.46 keV and width of 0.04 keV. The solid line fits the spectrum by a blackbody model.

data, a thorough understanding of the structure and evolution of the accreted matter in CVs could be reachable.

A rough estimation of the exposures could be done. For CVs within 50 pc, the typical 0.1-2 keV X-ray flux is $\sim 10^{-12}$ to $\sim 10^{-11}$ erg s $^{-1}$ cm $^{-2}$. **Simulation shows an HUBs snapshot of 10 to 100 ks (depending on the flux of the target) could provide a spectrum with sufficient photons for a targeted CV to identify the important emission lines (e.g., of the O and Ne elements) of one targeted CV for further investigation. A total sample of 30 bright CVs in the solar neighborhood requires 30 snapshots with** a total exposure of 1.4×10^6 s (16 days).

With the large effective area and high spectral resolution, HUBs can greatly improve our understanding on accretion process in CVs.

3.1.5 Stars

Stars located across almost all regions of a Hertzsprung–Russell diagram have been identified as X-ray sources, although with different mechanisms. Stellar magnetic corona is the predominant origin of X-rays for late type stars, while for massive and hot stars, the X-ray emission is from shocks forming in unstable winds. The X-ray radiation of pre-main sequence stars may originate both in hot coronal plasma or shocks [23].

Stellar magnetic activity provides substantial information on the magnetic dynamo and the coronal heating process. It is also of great value for exploring the interaction between stars and their planets and determining the habitable zone of different stars [23, 57]. Stellar magnetic activity is ubiquitous in late-type stars, which can be traced by various proxies, including spots and flares from photosphere, emission lines from chromosphere, and X-ray and radio emissions from corona. The activity level strongly depends on stellar parameters (e.g., stellar mass, age).

X-ray astronomy has played a key role in stellar activity studies. The X-ray luminosity of active stars in the quiet state ranges from 10^{27} to 10^{31} erg/s, while it is $1-2$ orders of magnitude brighter during flares [95, 23, 33]. It helps establish the famous activity-rotation relation (e.g., [73, 106]). In the relation, the X-ray activity is described as the ratio between X-ray luminosity and bolometric luminosity, while the Rossby number is used to trace stellar rotation, which is defined as the ratio of the rotation period to the convective turnover time. The relation is usually suggested to consist of two distinct sequences: the saturated region for rapidly rotating stars, in which the activity level keeps constant, and the power-law decay region for slowly rotating stars, where the activity level is rotation-dependent [106].

X-ray spectral observations have yielded a typical temperature of about $0.1-1$ keV for the stellar corona, belonging to the soft X-ray band. Previous studies using the low-resolution spectra (e.g., Chandra/ACIS, XMM-Newton/MOS) have measured the coronal temperatures and discussed the distribution of differential emission measures (dEM) for some nearby active stars [22]. High-resolution X-ray spectroscopy, on the other hand, is mainly done with Chandra/HETG and XMM-Newton/RGS high-resolution spectrometers. By using the He-like and H-like lines from different elements (e.g., C, N, O), the distributions of some physical parameters (e.g., coronal temperature and density, dEM, metallicity) during quiet states and flares have been well constrained for dozens of stars [95]. High-resolution spectra of active stars revealed a new trend that runs opposite to the solar FIP effect, called "inverse FIP (IFIP) effect" [68].

Although previous studies provide a number of surprising findings, there are many key issues unresolved. The standard picture of the activity-rotation relation has been challenged by recent studies, such as the variable activity level in the saturation region [78] and more sequences possibly divided in the relation [65]. It is also doubted that the distribution of coronal physical parameters are universal among stars due to the small and incomplete sample with high-resolution spectroscopic observations. For example, more than 900 F/G/K-type stars are located within 30 pc of the solar system [25], but only about 40 ones were observed; most stars around the solar system are M-type dwarfs, but only a few were observed (e.g., Proxima Cen [21] and CN Leo [50]). More importantly, some basic physical questions including the mechanism of the saturation and the connection between the relation and magnetic dynamo are poor understood. A large sample covering different types of stars, with well-measured activities and spectral parameters, can help investigate the physical properties of stellar magnetic dynamo and provide potential diagnostics of heating mechanisms.

HUBS can help establish a large high-resolution X-ray spectral sample for stars with different spectral types, rotation periods, ages, and metallicities. For single star, detailed diagnostics of the

coronal temperature and density can be done with the emission lines from different elements. With further investigation of the dEM, the FIP and IFIP effects, and the area of the active region, a comparison with the Sun can help explore the flare mechanism and heating process. On the other hand, by using the large sample, the distribution of these parameters and their relationships with different stellar parameters (e.g., mass, age, rotation) will help understand the structure and evolution of stars.

For typical active stars, an exposure of 100 ks by HUBS can obtain a spectrum with a sufficiently high signal-to-noise ratio for following studies; for close stars, the exposure time can be reduced to around 10–30 ks. Therefore, the exposure time of 100 stars is about 10^3 to 10^4 ks. **Taking Proxima Cen as an example, simulation shows that HUBS can clearly distinguish emission lines in its spectrum (typical for M-type active stars) compared with XMM-Newton/RGS observations with an exposure time of ≈800 s.**

With the large effective area and high spectral resolution, it can be predicted that HUBS will provide a valuable opportunity to advance stellar magnetic activity studies.

References

[1] Yuki Amano et al. "Evidence for Resonance Scattering in the X-Ray Grating Spectrum of the Supernova Remnant N49". In: *ApJ* 897.1, 12 (July 2020), p. 12. DOI: 10.3847/1538-4357/ab90fc. arXiv: 2005.04626 [astro-ph.HE].

[2] Rino Bandiera and Sidney van den Bergh. "Changes in the Optical Remnant of Kepler's Supernova during the Period 1942–1989". In: *ApJ* 374 (June 1991), p. 186. DOI: 10.1086/170108.

[3] Jayant Bhalerao et al. "X-Ray Ejecta Kinematics of the Galactic Core-Collapse Supernova Remnant G292.0+1.8". In: *ApJ* 800.1, 65 (Feb. 2015), p. 65. DOI: 10.1088/0004-637X/800/1/65. arXiv: 1408.1949 [astro-ph.HE].

[4] William P. Blair, Knox S. Long, and Olaf Vancura. "A Detailed Optical Study of Kepler's Supernova Remnant". In: *ApJ* 366 (Jan. 1991), p. 484. DOI: 10.1086/169583.

[5] William P. Blair, Ravi Sankrit, and John C. Raymond. "Hubble Space Telescope Imaging of the Primary Shock Front in the Cygnus Loop Supernova Remnant". In: *AJ* 129.5 (May 2005), pp. 2268–2280. DOI: 10.1086/429381.

[6] Sjors Broersen and Jacco Vink. "A Chandra X-ray study of the mixed-morphology supernova remnant 3C 400.2". In: *MNRAS* 446.4 (Feb. 2015), pp. 3885–3894. DOI: 10.1093/mnras/stu2119. arXiv: 1502.00642 [astro-ph.HE].

[7] V. Burwitz et al. "The Chandra LETGS high resolution X-ray spectrum of the isolated neutron star RX J1856.5-3754". In: *A&A* 379 (Nov. 2001), pp. L35–L38. DOI: 10.1051/0004-6361:20011304. arXiv: astro-ph/0109374 [astro-ph].

[8] Yang Chen et al. "Resonant Scattering Effect on the Soft X-Ray Line Emission from the Hot Interstellar Medium. I. Galactic Bulges". In: *ApJ* 861.2, 138 (July 2018), p. 138. DOI: 10.3847/1538-4357/aaca32. arXiv: 1806.01474 [astro-ph.GA].

[9] R. A. Chevalier, R. P. Kirshner, and J. C. Raymond. "The optical emission from a fast shock wave with application to supernova remnants." In: *ApJ* 235 (Jan. 1980), pp. 186–195. DOI: 10.1086/157623.

[10] Roger A. Chevalier and Jeffrey Oishi. "Cassiopeia A and Its Clumpy Presupernova Wind". In: *ApJL* 593.1 (Aug. 2003), pp. L23–L26. DOI: 10.1086/377572. arXiv: astro-ph/0306376 [astro-ph].

[11] A. Chiotellis, K. M. Schure, and J. Vink. "The imprint of a symbiotic binary progenitor on the properties of Kepler's supernova remnant". In: *A&A* 537, A139 (Jan. 2012), A139. DOI: 10.1051/0004-6361/201014754. arXiv: 1103.5487 [astro-ph.GA].

[12] L. R. Cominsky and K. S. Wood. "Discovery of a 7.1 hour period and eclipses from MXB 1659-29." In: *ApJ* 283 (Aug. 1984), pp. 765–773. DOI: 10.1086/162361.

[13] J. Cottam, F. Paerels, and M. Mendez. "Gravitationally redshifted absorption lines in the X-ray burst spectra of a neutron star". In: *Nature* 420.6911 (Nov. 2002), pp. 51–54. DOI: 10.1038/nature01159. arXiv: astro-ph/0211126 [astro-ph].

[14] Andrew Cumming and Lars Bildsten. "Carbon Flashes in the Heavy-Element Ocean on Accreting Neutron Stars". In: *ApJL* 559.2 (Oct. 2001), pp. L127–L130. DOI: 10.1086/323937. arXiv: astro-ph/0107213 [astro-ph].

[15] P. B. Demorest et al. "A two-solar-mass neutron star measured using Shapiro delay". In: *Nature* 467.7319 (Oct. 2010), pp. 1081–1083. DOI: 10.1038/nature09466. arXiv: 1010.5788 [astro-ph.HE].

[16] T. Ergin et al. "Recombining Plasma and Gamma-Ray Emission in the Mixed-morphology Supernova Remnant 3C 400.2". In: *ApJ* 842.1, 22 (June 2017), p. 22. DOI: 10.3847/1538-4357/aa72ee. arXiv: 1705.06442 [astro-ph.HE].

[17] Duncan K. Galloway and Laurens Keek. "Thermonuclear X-ray Bursts". In: *Astrophysics and Space Science Library*. Ed. by Tomaso M. Belloni, Mariano Méndez, and Chengmin Zhang. Vol. 461. Astrophysics and Space Science Library. Jan. 2021, pp. 209–262. DOI: 10.1007/978-3-662-62110-3_5. arXiv: 1712.06227 [astro-ph.HE].

[18] Duncan K. Galloway et al. "Discovery of a 552 Hz Burst Oscillation in the Low-Mass X-Ray Binary EXO 0748-676". In: *ApJL* 711.2 (Mar. 2010), pp. L148–L151. DOI: 10.1088/2041-8205/711/2/L148. arXiv: 0910.5546 [astro-ph.HE].

[19] Parviz Ghavamian et al. "Balmer-dominated Spectra of Nonradiative Shocks in the Cygnus Loop, RCW 86, and Tycho Supernova Remnants". In: *ApJ* 547.2 (Feb. 2001), pp. 995–1009. DOI: 10.1086/318408. arXiv: astro-ph/0010496 [astro-ph].

[20] Parviz Ghavamian et al. "The Detection of Far-Ultraviolet Line Emission from Balmer-Dominated Supernova Remnants in the Large Magellanic Cloud". In: *ApJ* 664.1 (July 2007), pp. 304–321. DOI: 10.1086/518686. arXiv: astro-ph/0703809 [astro-ph].

[21] M. Güdel et al. "Flares from small to large: X-ray spectroscopy of Proxima Centauri with XMM-Newton". In: *A&A* 416 (Mar. 2004), pp. 713–732. DOI: 10.1051/0004-6361:20031471. arXiv: astro-ph/0312297 [astro-ph].

[22] Manuel Güdel. "X-ray astronomy of stellar coronae". In: *A&A Rv* 12.2-3 (Sept. 2004), pp. 71–237. DOI: 10.1007/s00159-004-0023-2. arXiv: astro-ph/0406661 [astro-ph].

[23] Manuel Güdel and Yaël Nazé. "X-ray spectroscopy of stars". In: *A&A Rv* 17.3 (Sept. 2009), pp. 309–408. DOI: 10.1007/s00159-009-0022-4. arXiv: 0904.3078 [astro-ph.SR].

[24] Frank Haberl. "The magnificent seven: magnetic fields and surface temperature distributions". In: *Ap&SS* 308.1-4 (Apr. 2007), pp. 181–190. DOI: 10.1007/s10509-007-9342-x. arXiv: astro-ph/0609066 [astro-ph].

[25] Natalie R. Hinkel et al. "A Catalog of Stellar Unified Properties (CATSUP) for 951 FGK-Stars within 30 pc". In: *ApJ* 848.1, 34 (Oct. 2017), p. 34. DOI: 10.3847/1538-4357/aa8b0f. arXiv: 1709.04465 [astro-ph.SR].

[26] Hitomi Collaboration et al. "Measurements of resonant scattering in the Perseus Cluster core with Hitomi SXS". In: *PASJ* 70.2, 10 (Mar. 2018), p. 10. DOI: 10.1093/pasj/psx127. arXiv: 1710.04648 [astro-ph.HE].

[27] W. C. G. Ho et al. "Magnetic Hydrogen Atmosphere Models and the Neutron Star RX J1856.5-3754". In: *American Astronomical Society Meeting Abstracts*. Vol. 207. American Astronomical Society Meeting Abstracts. Dec. 2005, 198.03, p. 198.03.

[28] Tyler Holland-Ashford et al. "Comparing Neutron Star Kicks to Supernova Remnant Asymmetries". In: *ApJ* 844.1, 84 (July 2017), p. 84. DOI: 10.3847/1538-4357/aa7a5c. arXiv: 1705.08454 [astro-ph.HE].

[29] John P. Hughes, Ichizo Hayashi, and Katsuji Koyama. "ASCA X-Ray Spectroscopy of Large Magellanic Cloud Supernova Remnants and the Metal Abundances of the Large Magellanic Cloud". In: *ApJ* 505.2 (Oct. 1998), pp. 732–748. DOI: 10.1086/306202. arXiv: astro-ph/9802342 [astro-ph].

[30] Una Hwang, Robert Petre, and Kathryn A. Flanagan. "X-Ray-emitting Ejecta in Puppis A Observed with Suzaku". In: *ApJ* 676.1 (Mar. 2008), pp. 378–389. DOI: 10.1086/528925. arXiv: 0712.3208 [astro-ph].

[31] J. J. M. in 't Zand et al. "Chandra spectroscopy of Rapid Burster type-I X-ray bursts". In: *arXiv e-prints*, arXiv:1703.07221 (Mar. 2017), arXiv:1703.07221. arXiv: 1703.07221 [astro-ph.HE].

[32] Hiroshi Itoh and Kuniaki Masai. "The effect of a circumstellar medium on the X-ray emission of young remnants of type II supernovae." In: *MNRAS* 236 (Feb. 1989), pp. 885–899. DOI: 10.1093/mnras/236.4.885.

[33] C. P. Johnstone and M. Güdel. "The coronal temperatures of low-mass main-sequence stars". In: *A&A* 578, A129 (June 2015), A129. DOI: 10.1051/0004-6361/201425283. arXiv: 1505.00643 [astro-ph.SR].

[34] J. S. Kaastra and R. Mewe. "Optical depth effects in the X-ray emission from supernova remnants". In: *A&A* 302 (Oct. 1995), p. L13.

[35] Victoria M. Kaspi. "Recent progress on anomalous X-ray pulsars". In: *Ap&SS* 308.1-4 (Apr. 2007), pp. 1–11. DOI: 10.1007/s10509-007-9309-y. arXiv: astro-ph/0610304 [astro-ph].

[36] Tomoaki Kasuga et al. "Spatially Resolved RGS Analysis of Kepler's Supernova Remnant". In: *ApJ* 915.1, 42 (July 2021), p. 42. DOI: 10.3847/1538-4357/abff4f. arXiv: 2105.04235 [astro-ph.HE].

[37] S. Katsuda et al. "Discovery of Fast-Moving X-Ray-Emitting Ejecta Knots in the Oxygen-Rich Supernova Remnant Puppis A". In: *ApJ* 678.1 (May 2008), pp. 297–302. DOI: 10.1086/586891. arXiv: 0805.1369 [astro-ph].

[38] S. Katsuda et al. "Forward Shock Proper Motions of Kepler's Supernova Remnant". In: *ApJ* 689.1 (Dec. 2008), pp. 225–230. DOI: 10.1086/592376. arXiv: 0812.0339 [astro-ph].

[39] Satoru Katsuda and Hiroshi Tsunemi. "XMM-Newton observations across the Cygnus Loop from northeastern rim to southwestern rim". In: *Advances in Space Research* 41.3 (Jan. 2008), pp. 383–389. DOI: 10.1016/j.asr.2007.05.015.

[40] Satoru Katsuda et al. "Dynamics of X-Ray-emitting Ejecta in the Oxygen-rich Supernova Remnant Puppis A Revealed by the XMM-Newton Reflection Grating Spectrometer". In: *ApJ* 768.2, 182 (May 2013), p. 182. DOI: 10.1088/0004-637X/768/2/182. arXiv: 1303.6607 [astro-ph.HE].

[41] Satoru Katsuda et al. "High-resolution X-Ray Spectroscopy of the Galactic Supernova Remnant Puppis A with XMM-Newton/RGS". In: *ApJ* 756.1, 49 (Sept. 2012), p. 49. DOI: 10.1088/0004-637X/756/1/49. arXiv: 1209.5496 [astro-ph.HE].

[42] Satoru Katsuda et al. "Possible Charge-exchange X-ray Emission in the Cygnus Loop Detected with Suzaku". In: *ApJ* 730.1, 24 (Mar. 2011), p. 24. DOI: 10.1088/0004-637X/730/1/24. arXiv: 1103.1669 [astro-ph.HE].

[43] Miho Katsuragawa et al. "Suzaku X-ray observations of the mixed-morphology supernova remnant CTB 1". In: *PASJ* 70.6, 110 (Dec. 2018), p. 110. DOI: 10.1093/pasj/psy114. arXiv: 1810.05373 [astro-ph.HE].

[44] Masahiro T. Kawasaki et al. "ASCA Observations of the Supernova Remnant IC 443: Thermal Structure and Detection of Overionized Plasma". In: *ApJ* 572.2 (June 2002), pp. 897–905. DOI: 10.1086/340383. arXiv: astro-ph/0202484 [astro-ph].

[45] Wolfgang E. Kerzendorf et al. "A Reconnaissance of the Possible Donor Stars to the Kepler Supernova". In: *ApJ* 782.1, 27 (Feb. 2014), p. 27. DOI: 10.1088/0004-637X/782/1/27. arXiv: 1309.5964 [astro-ph.SR].

[46] Yosuke Koshiba et al. "High-resolution X-ray study of supernova remnant J0453.6-6829 with unusually high forbidden-to-resonance ratio". In: *PASJ* 74.4 (Aug. 2022), pp. 757–766. DOI: 10.1093/pasj/psac033. arXiv: 2204.09364 [astro-ph.HE].

[47] James M. Lattimer and Madappa Prakash. "Neutron star observations: Prognosis for equation of state constraints". In: *PhR* 442.1-6 (Apr. 2007), pp. 109–165. DOI: 10.1016/j.physrep.2007.02.003. arXiv: astro-ph/0612440 [astro-ph].

[48] N. A. Levenson et al. "Panoramic Views of the Cygnus Loop". In: *ApJS* 118.2 (Oct. 1998), pp. 541–561. DOI: 10.1086/313136. arXiv: astro-ph/9805008 [astro-ph].

[49] Jiang-Tao Li et al. "XMM-Newton large program on SN1006 - I. Methods and initial results of spatially resolved spectroscopy". In: *MNRAS* 453.4 (Nov. 2015), pp. 3953–3974. DOI: 10.1093/mnras/stv1882. arXiv: 1508.02950 [astro-ph.HE].

[50] C. Liefke, B. Fuhrmeister, and J. H. M. M. Schmitt. "Multiwavelength observations of a giant flare on CN Leonis. III. Temporal evolution of coronal properties". In: *A&A* 514, A94 (May 2010), A94. DOI: 10.1051/0004-6361/201014012. arXiv: 1003.4128 [astro-ph.SR].

[51] L. A. Lopez et al. "Typing Supernova Remnants Using X-Ray Line Emission Morphologies". In: *ApJL* 706.1 (Nov. 2009), pp. L106–L109. DOI: 10.1088/0004-637X/706/1/L106. arXiv: 0910.3208 [astro-ph.HE].

[52] Laura A. Lopez et al. "Using the X-ray Morphology of Young Supernova Remnants to Constrain Explosion Type, Ejecta Distribution, and Chemical Mixing". In: *ApJ* 732.2, 114 (May 2011), p. 114. DOI: 10.1088/0004-637X/732/2/114. arXiv: 1011.0731 [astro-ph.HE].

[53] K. Maeda et al. "Nucleosynthesis in Two-Dimensional Delayed Detonation Models of Type Ia Supernova Explosions". In: *ApJ* 712.1 (Mar. 2010), pp. 624–638. DOI: 10.1088/0004-637X/712/1/624. arXiv: 1002.2153 [astro-ph.SR].

[54] P. Maggi et al. "The population of X-ray supernova remnants in the Large Magellanic Cloud". In: *A&A* 585, A162 (Jan. 2016), A162. DOI: 10.1051/0004-6361/201526932. arXiv: 1509.09223 [astro-ph.HE].

[55] Pierre Maggi et al. "The supernova remnant population of the Small Magellanic Cloud". In: *A&A* 631, A127 (Nov. 2019), A127. DOI: 10.1051/0004-6361/201936583. arXiv: 1908.11234 [astro-ph.HE].

[56] D. Christopher Martin et al. "A turbulent wake as a tracer of 30,000years of Mira's mass loss history". In: *Nature* 448.7155 (Aug. 2007), pp. 780–783. DOI: 10.1038/nature06003.

[57] Kensuke Masui et al. "The Nature of Unresolved Soft X-Ray Emission from the Galactic Disk". In: *PASJ* 61 (Jan. 2009), S115. DOI: 10.1093/pasj/61.sp1.S115.

[58] Martin G. F. Mayer et al. "A global view of shocked plasma in the supernova remnant Puppis A provided by SRG/eROSITA". In: *A&A* 661, A31 (May 2022), A31. DOI: 10.1051/0004-6361/202142517. arXiv: 2110.12220 [astro-ph.HE].

[59] Sandro Mereghetti. "Pulsars and Magnetars". In: *Brazilian Journal of Physics* 43.5-6 (Dec. 2013), pp. 356–368. DOI: 10.1007/s13538-013-0137-y. arXiv: 1304.4825 [astro-ph.HE].

[60] Marco Miceli et al. "Collisionless shock heating of heavy ions in SN 1987A". In: *Nature Astronomy* 3 (Jan. 2019), pp. 236–241. DOI: 10.1038/s41550-018-0677-8. arXiv: 1901.10336 [astro-ph.HE].

[61] Dan Milisavljevic and Robert A. Fesen. "A Detailed Kinematic Map of Cassiopeia A's Optical Main Shell and Outer High-velocity Ejecta". In: *ApJ* 772.2, 134 (Aug. 2013), p. 134. DOI: 10.1088/0004-637X/772/2/134. arXiv: 1306.2310 [astro-ph.HE].

[62] Dan Milisavljevic and Robert A. Fesen. "The bubble-like interior of the core-collapse supernova remnant Cassiopeia A". In: *Science* 347.6221 (Jan. 2015), pp. 526–530. DOI: 10.1126/science.1261949. arXiv: 1501.07283 [astro-ph.HE].

[63] Matthew J. Millard et al. "An Ejecta Kinematics Study of Kepler's Supernova Remnant with High-resolution Chandra HETG Spectroscopy". In: *ApJ* 893.2, 98 (Apr. 2020), p. 98. DOI: 10.3847/1538-4357/ab7db1. arXiv: 1905.04475 [astro-ph.HE].

[64] Matthew J. Millard et al. "The 3D X-Ray Ejecta Structure of Tycho's Supernova Remnant". In: *ApJ* 937.2, 121 (Oct. 2022), p. 121. DOI: 10.3847/1538-4357/ac8f30. arXiv: 2209.01632 [astro-ph.HE].

[65] M. Mittag, J. H. M. M. Schmitt, and K. -P. Schröder. "Revisiting the connection between magnetic activity, rotation period, and convective turnover time for main-sequence stars". In: *A&A* 618, A48 (Oct. 2018), A48. DOI: 10.1051/0004-6361/201833498. arXiv: 1807.05825 [astro-ph.SR].

[66] K. Mukai et al. "Two Types of X-Ray Spectra in Cataclysmic Variables". In: *The Astrophysical Journal* 586.1 (Mar. 2003), pp. L77–L80. DOI: 10.1086/374583. URL: https://doi.org/10.1086/374583.

[67] Ken'ichi Nomoto et al. "Nucleosynthesis yields of core-collapse supernovae and hypernovae, and galactic chemical evolution". In: *NuPhA* 777 (Oct. 2006), pp. 424–458. DOI: 10.1016/j.nuclphysa.2006.05.008. arXiv: astro-ph/0605725 [astro-ph].

[68] R. Nordon and E. Behar. "Abundance variations and first ionization potential trends during large stellar flares". In: *A&A* 482.2 (May 2008), pp. 639–651. DOI: 10.1051/0004-6361:20078848. arXiv: 0712.0482 [astro-ph].

[69] A. A. Nucita et al. "The puzzling symbiotic X-ray system 4U1700+24". In: *A&A* 562, A55 (Feb. 2014), A55. DOI: 10.1051/0004-6361/201322680. arXiv: 1401.2053 [astro-ph.HE].

[70] Takao Ohnishi et al. "X-Ray Spectrum of a Peculiar Supernova Remnant, G359.1-0.5". In: *PASJ* 63 (June 2011), p. 527. DOI: 10.1093/pasj/63.3.527. arXiv: 1103.0348 [astro-ph.HE].

[71] Feryal Özel and Paulo Freire. "Masses, Radii, and the Equation of State of Neutron Stars". In: *ARA&A* 54 (Sept. 2016), pp. 401–440. DOI: 10.1146/annurev-astro-081915-023322. arXiv: 1603.02698 [astro-ph.HE].

[72] Dirk Pandel et al. "X-Ray Observations of the Boundary Layer in Dwarf Novae at Low Accretion Rates". In: *The Astrophysical Journal* 626.1 (June 2005), pp. 396–410. DOI: 10.1086/429983. URL: https://doi.org/10.1086/429983.

[73] N. Pizzolato et al. "The stellar activity-rotation relationship revisited: Dependence of saturated and non-saturated X-ray emission regimes on stellar mass for late-type dwarfs". In: *A&A* 397 (Jan. 2003), pp. 147–157. DOI: 10.1051/0004-6361:20021560.

[74] Gabriele Ponti et al. "Measuring masses in low mass X-ray binaries via X-ray spectroscopy: the case of MXB 1659-298". In: *MNRAS* 481.1 (Nov. 2018), pp. L94–L99. DOI: 10.1093/mnrasl/sly120. arXiv: 1807.04757 [astro-ph.HE].

[75] A. Rasmussen, E. Behar, and J. Vink. "High resolution X-ray spectroscopy of SNRs in the Magellanic Clouds". In: *34th COSPAR Scientific Assembly*. Vol. 34. Jan. 2002, 3040, p. 3040.

[76] A. P. Rasmussen et al. "The X-ray spectrum of the supernova remnant 1E 0102.2−7219". In: *A&A* 365 (Jan. 2001), pp. L231–L236. DOI: 10.1051/0004-6361:20000231.

[77] T. Rauch, V. Suleimanov, and K. Werner. "Absorption features in the spectra of X-ray bursting neutron stars". In: *A&A* 490.3 (Nov. 2008), pp. 1127–1134. DOI: 10.1051/0004-6361:200810129. arXiv: 0809.2170 [astro-ph].

[78] A. Reiners, M. Schüssler, and V. M. Passegger. "Generalized Investigation of the Rotation-Activity Relation: Favoring Rotation Period instead of Rossby Number". In: *ApJ* 794.2, 144 (Oct. 2014), p. 144. DOI: 10.1088/0004-637X/794/2/144. arXiv: 1408.6175 [astro-ph.SR].

[79] Stephen P. Reynolds et al. "A Deep Chandra Observation of Kepler's Supernova Remnant: A Type Ia Event with Circumstellar Interaction". In: *ApJL* 668.2 (Oct. 2007), pp. L135–L138. DOI: 10.1086/522830. arXiv: 0708.3858 [astro-ph].

[80] Shawn R. Roberts and Q. Daniel Wang. "X-ray emission from charge exchange in the Cygnus Loop SNR". In: *MNRAS* 449.2 (May 2015), pp. 1340–1346. DOI: 10.1093/mnras/stv319. arXiv: 1502.05068 [astro-ph.HE].

[81] Pilar Ruiz-Lapuente. "The Light Curve and Distance of the Kepler Supernova: News from Four Centuries Ago". In: *ApJ* 842.2, 112 (June 2017), p. 112. DOI: 10.3847/1538-4357/aa6f09. arXiv: 1612.07399 [astro-ph.SR].

[82] Pilar Ruiz-Lapuente et al. "The binary progenitor of Tycho Brahe's 1572 supernova". In: *Nature* 431.7012 (Oct. 2004), pp. 1069–1072. DOI: 10.1038/nature03006. arXiv: astro-ph/0410673 [astro-ph].

[83] Makoto Sawada and Katsuji Koyama. "X-Ray Observations of the Supernova Remnant W28 with Suzaku. I. Spectral Study of the Recombining Plasma". In: *PASJ* 64, 81 (Aug. 2012), p. 81. DOI: 10.1093/pasj/64.4.81. arXiv: 1202.3125 [astro-ph.HE].

[84] S. Sazonov et al. "X-ray luminosity function of faint point sources in the Milky Way". In: *A&A* 450.1 (Apr. 2006), pp. 117–128. DOI: 10.1051/0004-6361:20054297. arXiv: astro-ph/0510049 [astro-ph].

[85] Ivo R. Seitenzahl et al. "Three-dimensional delayed-detonation models with nucleosynthesis for Type Ia supernovae". In: *MNRAS* 429.2 (Feb. 2013), pp. 1156–1172. DOI: 10.1093/mnras/sts402. arXiv: 1211.3015 [astro-ph.SR].

[86] J. Sollerman et al. "High resolution spectroscopy of Balmer-dominated shocks in the RCW 86, Kepler and SN 1006 supernova remnants". In: *A&A* 407 (Aug. 2003), pp. 249–257. DOI: 10.1051/0004-6361:20030839. arXiv: astro-ph/0306196 [astro-ph].

[87] Andrew W. Steiner, James M. Lattimer, and Edward F. Brown. "The Neutron Star Mass-Radius Relation and the Equation of State of Dense Matter". In: *ApJL* 765.1, L5 (Mar. 2013), p. L5. DOI: 10.1088/2041-8205/765/1/L5. arXiv: 1205.6871 [nucl-th].

[88] R. Sturm et al. "High resolution X-ray spectroscopy of SN 1987 A: monitoring with XMM-Newton". In: *A&A* 515, A5 (June 2010), A5. DOI: 10.1051/0004-6361/200913317. arXiv: 1002.1865 [astro-ph.HE].

[89] Tuguldur Sukhbold et al. "Core-collapse Supernovae from 9 to 120 Solar Masses Based on Neutrino-powered Explosions". In: *ApJ* 821.1, 38 (Apr. 2016), p. 38. DOI: 10.3847/0004-637X/821/1/38. arXiv: 1510.04643 [astro-ph.HE].

[90] Lei Sun and Yang Chen. "An XMM-Newton X-Ray View of Supernova Remnant W49B: Revisiting Its Recombining Plasmas and Progenitor Type". In: *ApJ* 893.2, 90 (Apr. 2020), p. 90. DOI: 10.3847/1538-4357/ab8001. arXiv: 2003.07237 [astro-ph.HE].

[91] Lei Sun and Yang Chen. "Spatially Resolved X-Ray Spectroscopy of Kepler's Supernova Remnant: Distinct Properties of the Circumstellar Medium and the Ejecta". In: *ApJ* 872.1, 45 (Feb. 2019), p. 45. DOI: 10.3847/1538-4357/aafb73. arXiv: 1901.07365 [astro-ph.HE].

[92] Lei Sun et al. "The Post-impact Evolution of the X-Ray-emitting Gas in SNR 1987A as Viewed by XMM-Newton". In: *ApJ* 916.1, 41 (July 2021), p. 41. DOI: 10.3847/1538-4357/ac033d. arXiv: 2103.03844 [astro-ph.HE].

[93] Hitomi Suzuki et al. "Plasma Diagnostics of the Supernova Remnant N132D using Deep XMM-Newton Observations with the Reflection Grating Spectrometer". In: *ApJ* 900.1, 39 (Sept. 2020), p. 39. DOI: 10.3847/1538-4357/aba524. arXiv: 2007.06158 [astro-ph.HE].

[94] Yukiko Tanaka et al. "Charge Exchange X-Ray Emission Detected in Multiple Shells of Supernova Remnant G296.1-0.5". In: *ApJ* 933.1, 101 (July 2022), p. 101. DOI: 10.3847/1538-4357/ac738f. arXiv: 2205.10038 [astro-ph.HE].

[95] Paola Testa, Jeremy J. Drake, and Giovanni Peres. "The Density of Coronal Plasma in Active Stellar Coronae". In: *ApJ* 617.1 (Dec. 2004), pp. 508–530. DOI: 10.1086/422355. arXiv: astro-ph/0405019 [astro-ph].

[96] Andrea Tiengo et al. "A variable absorption feature in the X-ray spectrum of a magnetar". In: *Nature* 500.7462 (Aug. 2013), pp. 312–314. DOI: 10.1038/nature12386. arXiv: 1308.4987 [astro-ph.HE].

[97] Danny Tsebrenko and Noam Soker. "Type Ia supernovae inside planetary nebulae: shaping by jets". In: *MNRAS* 435.1 (Oct. 2013), pp. 320–328. DOI: 10.1093/mnras/stt1301. arXiv: 1305.1845 [astro-ph.SR].

[98] Hiroshi Tsunemi et al. "The Plasma Structure of the Cygnus Loop from the Northeastern Rim to the Southwestern Rim". In: *ApJ* 671.2 (Dec. 2007), pp. 1717–1725. DOI: 10.1086/523263. arXiv: 0710.1135 [astro-ph].

[99] H. Uchida et al. "High Forbidden-to-resonance Line Ratio of O VII Discovered from the Cygnus Loop". In: *ApJ* 871.2, 234 (Feb. 2019), p. 234. DOI: 10.3847/1538-4357/aaf8a6. arXiv: 1812.06616 [astro-ph.HE].

[100] Hiroyuki Uchida et al. "Recombining Plasma and Hard X-Ray Filament in the Mixed-Morphology Supernova Remnant W 44". In: *PASJ* 64, 141 (Dec. 2012), p. 141. DOI: 10.1093/pasj/64.6.141. arXiv: 1208.0113 [astro-ph.HE].

[101] Matthew van Adelsberg et al. "Spatial Structure and Collisionless Electron Heating in Balmer-dominated Shocks". In: *ApJ* 689.2 (Dec. 2008), pp. 1089–1104. DOI: 10.1086/592680. arXiv: 0803.2521 [astro-ph].

[102] J. Vink, J. S. Kaastra, and J. A. M. Bleeker. "A new mass estimate and puzzling abundances of SNR Cassiopeia A." In: *A&A* 307 (Mar. 1996), pp. L41–L44.

[103] Jacco Vink. "Supernova remnants: the X-ray perspective". In: *A&A Rv* 20, 49 (Dec. 2012), p. 49. DOI: 10.1007/s00159-011-0049-1. arXiv: 1112.0576 [astro-ph.HE].

[104] Jacco Vink et al. "The Slow Temperature Equilibration behind the Shock Front of SN 1006". In: *ApJL* 587.1 (Apr. 2003), pp. L31–L34. DOI: 10.1086/375125. arXiv: astro-ph/0303051 [astro-ph].

[105] Weiyang Wang et al. "The Optical/UV Excess of X-Ray-dim Isolated Neutron Stars. I. Bremsstrahlung Emission from a Strangeon Star Atmosphere". In: *ApJ* 837.1, 81 (Mar. 2017), p. 81. DOI: 10.3847/1538-4357/aa5e52. arXiv: 1603.08288 [astro-ph.HE].

[106] Nicholas J. Wright et al. "The Stellar-activity-Rotation Relationship and the Evolution of Stellar Dynamos". In: *ApJ* 743.1, 48 (Dec. 2011), p. 48. DOI: 10.1088/0004-637X/743/1/48. arXiv: 1109.4634 [astro-ph.SR].

[107] Lai Xiaoyu and Xu Renxin. "Strangeon and Strangeon Star". In: *Journal of Physics Conference Series*. Vol. 861. Journal of Physics Conference Series. June 2017, 012027, p. 012027. DOI: 10.1088/1742-6596/861/1/012027. arXiv: 1701.08463 [astro-ph.HE].

[108] H. Xu et al. "High-Resolution Observations of the Elliptical Galaxy NGC 4636 with the Reflection Grating Spectrometer on Board XMM-Newton". In: *ApJ* 579.2 (Nov. 2002), pp. 600–606. DOI: 10.1086/342828. arXiv: astro-ph/0110013 [astro-ph].

[109] Ren-Xin Xu. "A solution to the puzzling symbiotic X-ray system 4U 1700+24". In: *Research in Astronomy and Astrophysics* 14.6, 617-624 (June 2014), pp. 617–624. DOI: 10.1088/1674-4527/14/6/001. arXiv: 1402.1290 [astro-ph.HE].

[110] H. Yamaguchi et al. "Discovery of Strong Radiative Recombination Continua from the Supernova Remnant IC 443 with Suzaku". In: *ApJL* 705.1 (Nov. 2009), pp. L6–L9. DOI: 10.1088/0004-637X/705/1/L6. arXiv: 0909.3848 [astro-ph.HE].

[111] Shigeo Yamauchi, Masayoshi Nobukawa, and Katsuji Koyama. "A systematic comparison of ionization temperatures between ionizing and recombining plasmas in supernova remnants". In: *PASJ* 73.3 (June 2021), pp. 728–734. DOI: 10.1093/pasj/psab033. arXiv: 2104.02375 [astro-ph.HE].

[112] Gao-Yuan Zhang et al. "Nonequilibrium Ionization in Mixed-morphology Supernova Remnants". In: *ApJ* 875.2, 81 (Apr. 2019), p. 81. DOI: 10.3847/1538-4357/ab0f9a. arXiv: 1902.10718 [astro-ph.HE].

[113] Shuang-Nan Zhang, Jinyuan Liao, and Yangsen Yao. "Measuring the black hole masses in accreting X-ray binaries by detecting the Doppler orbital motion of their accretion disc wind absorption lines". In: *MNRAS* 421.4 (Apr. 2012), pp. 3550–3556. DOI: 10.1111/j.1365-2966.2012.20579.x. arXiv: 1201.3451 [astro-ph.HE].

[114] Svetozar A. Zhekov et al. "High-Resolution X-Ray Spectroscopy of SNR 1987A: Chandra Letg and HETG Observations in 2007". In: *ApJ* 692.2 (Feb. 2009), pp. 1190–1204. DOI: 10.1088/0004-637X/692/2/1190. arXiv: 0810.5313 [astro-ph].

[115] Ping Zhou and Jacco Vink. "Asymmetric Type-Ia supernova origin of W49B as revealed from spatially resolved X-ray spectroscopic study". In: *A&A* 615, A150 (July 2018), A150. DOI: 10.1051/0004-6361/201731583. arXiv: 1707.05107 [astro-ph.HE].

[116] Ping Zhou et al. "Expanding Molecular Bubble Surrounding Tyco's Supernova Remnant (SN 1572) Observed with the IRAM 30 m Telescope: Evidence for a Single-degenerate Progenitor". In: *ApJ* 826.1, 34 (July 2016), p. 34. DOI: 10.3847/0004-637X/826/1/34. arXiv: 1605.01284 [astro-ph.GA].

[117] Xin Zhou et al. "Unveiling the spatial structure of the overionized plasma in the supernova remnant W49B". In: *MNRAS* 415.1 (July 2011), pp. 244–250. DOI: 10.1111/j.1365-2966.2011.18695.x. arXiv: 1103.2290 [astro-ph.HE].